11/03/2025

Hothouse hydrology: Evolving river dynamics in the Eocene Montllobat and Castissent Formations, Southern Pyrenees

Jonah S. McLeod*[1,2], Alexander C. Whittaker[1], Gary J. Hampson[1], Rebecca E. Bell[1], Marine Prieur[3], Oliver G. Fuller-Field[1], Luis Valero[4], Xiang Yan[1], Jeffery M. Valenza[5]

1 Department of Earth Science and Engineering, Imperial College London, London SW7 2AZ, UK

2 Grantham Institute, Science and Solutions for a Changing Planet DTP, Exhibition Road, South Kensington, London SW7 2AZ, UK

3 Department of Earth Sciences, University of Geneva, 1205 Geneva, Switzerland

4 Departament de Dinàmica de la Terra i de l'Oceà, Faculty of Earth Science, University of Barcelona, Martí i Franquès s/n, 08028 Barcelona, Spain

5 Department of Geography, University of California, Santa Barbara, 1832 Ellison Hall, Santa Barbara, CA, 93106, USA

ABSTRACT

Environmental forcings have shaped landscapes and basins across geologic history, and Earth's surface is projected to undergo rapid change in the near future amidst increasing climate extremes. Rivers are highly sensitive to climate and tectonic change, and understanding how fluvial systems respond to greenhouse climates in dynamic tectono-geomorphic settings is vital to projecting imminent landscape change in the face of global warming. We look to the southern Pyrenean Tremp-Graus basin during the Early Eocene Climatic Optimum (EECO), analogous to future anthropogenic climate scenarios. We focus specifically on the fluvial deposits of the Montllobat and Castissent formations, formed during the early Pyrenean orogeny. This succession records a unique shift in geomorphology and a 20 km progradation of the shoreline and its feeder rivers in < 0.8 Myrs. Using field-based quantitative palaeohydrology, we reconstruct the evolving morphometry and hydrodynamics of ancient river systems in a foreland basin. The transition from the Montllobat Fm. into the Castissent Fm. at c. 50.5 Ma is associated with a sharp change in palaeohydraulics: a statistically significant reduction in cross-set height, a 1.4-fold increase in channel slope, a 40% increase in water discharge, and a 15% increase in total sediment flux. This intensification in hydrological regime implies a clear climate driver, and is compounded with a shift in fluvial planform morphology: we interpret a switch from anastomosing to a dominantly braided planform at the onset of the Castissent interval. We suggest the transient hydrological signature of the Castissent Fm. was driven by Ypresian hyperthermal events superimposed on a levelling-off in the global cooling trend at the end of the EECO, and an increase in tectonic uplift rates c. 50 Ma. This analysis holistically reconstructs the dynamics of ancient rivers in the Eocene hothouse, and in conjunction with isotope and exhumation records, reveals the potential to extract complex tectono-climatic signals from fluvial stratigraphy.

Keywords

Sedimentology, stratigraphy, palaeohydrology, landscape dynamics

INTRODUCTION

Across Earth's history, landscapes and basins have responded to climate and tectonic forcing (Armitage *et al.*, 2011; Whittaker, 2012; Romans *et al.*, 2016a). In today's warming world, multiple landscape systems are thought to be on the edge of marked geomorphic change (Flannigan *et al.*, 2006; Gariano & Guzzetti, 2016; IPCC, 2022; McLeod *et al.*, 2024) owing to increasing weather extremes worldwide (IPCC, 2022). In particular, rivers are one of the most significant drivers of landscape evolution (Romans *et al.*, 2016a), transporting 10^{10} tonnes of material across the Earth's surface each year (Milliman & Meade, 1983), and are documented to be highly sensitive to climate and weather patterns. While we cannot directly study landscape response to future environmental or tectonic change, we can collect observational data of geomorphic and sedimentary responses to past climate and tectonic change. Consequently, fluvial stratigraphy can be used as an archive of river response to past boundary condition change, meaning we can turn to the past to inform projections of future landscape change (e.g., Armitage et al., 2011; Fielding et al., 2018; Lyster et al., 2020; Lyster, Whittaker, Hajek, et al., 2022; McLeod et al., 2023, 2024; Sharma et al., 2023; Whittaker, 2012).

Understanding the climate of the past has increasingly become possible in recent years using geochemical proxies of weathering, temperature and precipitation, mostly in marine settings but increasingly in the continental sedimentary record (Honegger *et al.*, 2020; Jaimes-Gutierrez *et al.*, 2024). Mountain belts are areas where rivers and continental processes may be particularly sensitive to climate change (IPCC, 2022), so the stratigraphic record of surface processes in mountainous regions could be especially valuable in deciphering the landscape dynamics of the past. Floodplain sediment and palaeosols already present a useful repository of these preserved environmental signals on the continents. However, river channels are more dynamic settings, and whilst they do record landscape change, disentangling climatic from tectonic information is challenging, and this is the focus of ongoing research (Armitage *et al.*, 2011; McLeod *et al.*, 2023, 2024; Sharma *et al.*, 2023; Prieur *et al.*, 2024; Rezwan *et al.*, 2025).

Facies-based sedimentological analysis of fluvial stratigraphy can yield important insights on the behaviour of ancient rivers in response to external drivers (e.g., Fielding et al., 2018; McLeod et al., 2023; Plink-Bjorklund, 2015). However, robust quantitative constraints on palaeohydrology are essential for extracting detailed insights on the sensitivity of landscapes to climate and tectonic change, and in doing so, using the past to inform understanding of landscape change in the present and future. There is now a wealth of techniques available for reconstructing the hydrology of rivers in the geologic past (e.g., Bradley & Venditti, 2017; Leclair & Bridge, 2001; Long, 2021; Lyster et al., 2023; Manning et al., 1890; Parker, 1976; Trampush et al., 2014; Wood et al., 2022), many of which are based on measurements of primary geologic observables in stratigraphy such as grain-size; bedform size and preservation (e.g. dune cross-set heights); and stratigraphic architecture (e.g. to reconstruct channel morphology and migration). Scaling relations developed by Bradley & Venditti (2017) and Leclair & Bridge (2001) based on field and laboratory data, as well as theoretical considerations, permit reconstruction of river flow depths from dune-cross-sets. Experimental insights on bedform evolution (e.g., Das et al., 2022) present opportunities to interpret flow stage from preserved river deposits. Lyster, Whittaker & Hajek (2022) built on Parker's (1976) use of planform stability fields to constrain river planform geometry using quantitative palaeohydrologic reconstructions in the rock record, with new comparisons to modern river datasets. Advances such as these are expanding our capacity for extracting environmental signals from ancient geomorphic systems (Romans *et al.*, 2016b; Lyster, 2022).

In this paper we address the challenge of extracting competing climatic and tectonic signals from fluvial channel stratigraphy. We use quantitative geologic techniques to reconstruct the evolving morphometry, transport dynamics and planform style of the well-documented Castissent and Montllobat Formations located in the Pyrenean mountains of Spain for the first time, and we evaluate how they compare to modern and geologic analogues. In doing so, we capture the geomorphic response of ancient rivers to the evolving climate and tectonics of the early Pyrenees during the hottest period of the Cenozoic (Westerhold *et al.*, 2020; IPCC, 2022).

GEOLOGIC BACKGROUND

The fluvial successions of the lower Eocene in the south-central unit of the southern Pyrenees of Spain offer extensive outcrop exposure within the dynamic setting of the growing Pyrenean orogen (e.g., Cabello et al., 2018; Marzo et al., 1988; Nijman & Puigdefàbregas, 1977), and record fluvial deposition during the Early Eocene Climatic Optimum (EECO), a global greenhouse period which represents the climax of the 9 million-year-long Eocene Hothouse. The EECO also has a number of hyperthermal events superimposed on it – these represent brief periods of pronounced global warming, considered anomalous when compared to typical conditions during this time interval.

During the early Pyrenean orogenesis, runoff flowed south into foreland sub-basins bound by imbricate thrusts, and rivers deflected westwards where they deposited a westward-thinning wedge of fluvio-deltaic, clastic sediment known as the Montanyana Group (Nijman & Nio, 1975). The best preserved units in the Montanyana succession are the Lower and Middle Montanyana Groups (LM, MM, Nijman, 1998), and in the fluvial domain (Tremp-Graus sub-basins) these comprise the Montllobat (Mlb) and Castissent (Cst) formations (Ypresian), respectively (Fig. 1). The rivers of the Montllobat and Castissent formations deposited continental sediment NW into an elongate bay, connected to the Atlantic (Juvany *et al.*, 2024), forming the Montanyana delta. The later Upper Montanyana Group (UM) sediments are similar in facies to the LM Group (Nijman, 1998).

The Montllobat and Castissent formations crop out across the Spanish Pyrenees in the Tremp-Graus basin in Catalonia and Aragon, and have been the focus of facies-based sedimentological investigation since the mid-1970s (e.g., Nijman & Nio, 1975; Nijman & Puigdefàbregas, 1977). The Castissent Formation forms a regional marker unit with a total thickness of 50 – 100 m and represents a strong progradational episode, which saw the shoreline and rivers of the clastic wedge prograde 20 km over the underlying Montllobat Fm. (and its shallow marine equivalent, the Castigaleu Fm.) for an estimated duration of 800 kyrs (Honegger *et al.*, 2020). Due to this distinctive progradation, excellent outcrop preservation, and its use as a reservoir analogue including its down-system genetic equivalents (Clark & Pickering, 1996; Puig *et al.*, 2019), the sandstones of the Castissent Formation have received more focus than other units in the continental Montanyana Group. It has been suggested that this progradation could be attributed to an increase in hinterland exhumation rate (Curry et al., 2021; Whitchurch et al., 2011 Fig. 2) and/or a possible change in climate or sea-level (Nijman, 1998; Honegger *et al.*, 2020).

The climate of the Castissent interval in particular is becoming increasingly quantified, as Honegger at al. (2020) used isotopic and geochemical signatures preserved in floodplain sediment and palaeosols to identify climate change during a hyperthermal event. They identify a carbon isotopic excursion (CIE) at c. 50 Ma as Eocene hyperthermal "U" (Fig. 2), associated with enrichment in immobile Ti, Zr and Al. Based on the CaO/Al_2O_3 ratios of the bulk palaeosol material, the average climate is reconstructed to have been sub-arid with a mean annual precipitation (MAP) of 376 mm/a, increasing to as high as 754 mm/a during CIEs. $\delta^{13}C$ records of benthic carbonates (Westerhold *et al.*, 2017; Honegger *et al.*, 2020) also show that Castissent deposition coincides with a levelling-off in a long-wavelength trend of global cooling (Fig. 2). Insights like this are helping to complete the picture of changing climate towards the end of the EECO, and suggest Montllobat and Castissent rivers were subject to tectono-climatic perturbations that have geologic preservation potential.

Marzo et al. (1988) mapped and logged the Castissent Fm. in some detail and described three multistorey sandsheet complexes, each described as a Member of the Castissent Formation (Fig. 3A). These sandsheet complexes are attributed to three successive fluvial systems separated by marine incursions and preserved floodplain deposits. Nijman (1998) identified the Castissent Formation as equivalent to the Middle Montanyana (MM) Megasequence, containing three Sequences (MMI, MMII and MMIII) which correspond to Castissent Members A, B and C (Marzo et al., 1988), respectively. Channel-fill bodies are vertically and laterally amalgamated, sand-rich and have a distinctive white-weathering and rounded exposure pattern (Fig. 4D-E). The Castissent has previously been interpreted as a braided system due to its sheet-like and predominantly multistorey, multilateral architectural style (Nijman & Nio, 1975). It is correlated westwards with the deep-water turbidites of the Arro and Fosado formations in the Ainsa Basin (Mutti & Sgavetti, 1987) and tentatively with the Torla and Broto systems in the Hecho Group of the Jaca basin (Caja *et al.*, 2010; Cornard & Pickering, 2020).

Whilst the Castissent interval lasted c. 0.8 Ma, the underlying Montllobat Fm. formed over approximately 2.5 Ma, and represents the first major phase of NW-oriented fluvial drainage in the Pyrenean foreland. The Montllobat Fm. comprises variably isolated and amalgamated, channelised sandstone and conglomerate bodies encased in mudstone-dominated, mottled floodplain deposits (Cabello *et al.*, 2018) with a total thickness of 150 – 250 m. The Montllobat Fm. has been interpreted to contain deposits of both meandering rivers, with prominent point-bar deposits (Van Eden, 1970; Nijman & Nio, 1975; Cabello *et al.*, 2018), and sheetflood-dominated river systems (Van der Meulen, 1989). The Lower Montanyana Group (Montllobat Fm.) comprises two Megasequences, the Lower LM (LLM) and Upper LM (ULM), separated by a Megasequence boundary associated with southward progradation of coarse alluvial fan sediment and an extensive conglomerate unit (Nijman, 1998), mapped by the Catalan geologic survey (ICC) on their Espills (1:2500; 251-2-2) sheet as conglomerate unit C3 (Picart *et al.*, 2010). We treat this Megasequence boundary as the boundary between two Members of the Montllobat Formation, which we describe here as Montllobat A (MlbA) and Montllobat B (MlbB).

Figure 3A summarises the stratigraphic framework used for this work: the Montllobat Fm. is equivalent to the LM Group, and its two Megasequences (LLM and ULM) are here labelled as Members MlbA and MlbB, respectively. The Middle Montanyana (MM) Group comprises one Megasequence, the Castissent Sandstone, and is subdivided into Members CstA, CstB and CstC (Marzo et al., 1988), each representing a full stratigraphic sequence. See Table S1 for further explanation.

These units are stratigraphic exemplars of the interplay between climate and tectonics in ancient geomorphic systems: hyperthermal events superimposed on a long-term cooling trend from the EECO competed with tectonic change in the early Pyrenees. High-frequency climate signals are becoming more widely interpreted in the continental rock record (McInerney & Wing, 2011; Turner, 2018; Rush *et al.*, 2021; Prieur *et al.*, 2024), including in the Castissent Formation, where indicators of climate change are preserved in floodplain sediment (Honegger at al., 2020). These units offer an excellent opportunity to quantify palaeohydrological changes in a well-defined tectonic and climatic context. In particular, we aim to use the dynamic channel deposits of ancient rivers to shed new light on the response of fluvial hydrology to environmental and/or tectonic signals in the past, and to reconstruct the sensitivity of palaeo-landscapes to known boundary condition changes.

METHODS

Field Data

Field data were collected at 42 sites in the Castissent and Montllobat Formations (Fig. 1). Primary numerical field observations (Fig. 4) included grain-size, the thickness and lee-face orientation of cross-sets, and the thickness, length, and accretion orientation of barforms. These primary field observations are collected in the context of previous studies of facies analysis and stratigraphic architecture in the Castissent and Montllobat Formations (Marzo *et al.*, 1988; Nijman, 1998; Cabello *et al.*, 2018; Puig *et al.*, 2019). Our field methodological approach for reconstructing palaeohydrology follows an approach which has been tested in various geologic settings recently (e.g., Ganti et al., 2019; Lyster et al., 2020; Wood et al., 2022) and is summarised below.

Cross-sets, the preserved remnants of river dunes, can be generally expected to scale in size with river flow depth (e.g., Bradley & Venditti, 2017). To estimate mean cross-set thickness, h_{xs}, from fluvial sediment, which are used in our reconstructions below, we obtained full thickness distributions from 1553 thickness measurements across 147 cross-sets, by measuring thickness along the major axis of a cross-set at 10-15 regular intervals (with a mean of N = 10.6 measurements per cross-set, cf. Lyster et al., 2022; McLeod et al., 2023). A scaling factor between mean and maximum cross-set thickness was calculated based on these data, so that our larger data set of maximum cross-set thicknesses in the two formations could be incorporated within our analysis (N = 1539). Accordingly, we used N = 1686 cross-set thickness measurements for palaeohydrological reconstruction across the Montllobat and Castissent Formations.

Where cross-set thickness distributions were obtained, we also measured median grain-size (D_{50}) and lee face orientation. Where grains were < 2 mm in diameter, D_{50} was estimated using the Wentworth scheme (Wentworth, 1922), and in conglomeratic bodies in which $D_{50} \geq 2$ mm, grain size distributions were measured according to the Wolman point-count method (Wolman, 1954), allowing reconstruction of maximum formative flow according to average bedload material grade. Cross-set lee-face orientations (N = 856) were measured and restored to palaeo-horizontal using measurements of regional structural dip in Stereonet 11 (Allmendinger *et al.*, 2013). Restored lee-face measurements were used in reconstructions of palaeocurrent direction and planform morphology.

Preserved barforms were recognised in the field by their sloping bar-accretion surfaces, often accompanied by superimposed dune-scale cross-stratification, following the approach of Chamberlain and Hajek (2018). The heights of barform accretion sets and channel-fill bodies (N = 221) were measured using a TruPulse laser range finder to provide further constraints on flow depth. Barform accretion surface orientations (N = 703) were measured using the same methodology as cross-set lee faces in order to determine accretion direction and bar mode – whether bars migrate downstream, laterally, or upstream relative to flow direction – sampling accretion surfaces at their steepest dip angle relative to structural bedding.

Analytical Workflow

The primary field data were processed using a quantitative palaeohydrological workflow based on a suite of theoretical numerical models, experimental relations and field observations. This methodological workflow is summarised in Figure 5. All uncertainty has been propagated through this workflow using Monte Carlo simulations with 10^6 runs, incorporating random distributions between uncertainty limits, following established methods (Ganti *et al.*, 2019; Lyster *et al.*, 2021; McLeod *et al.*, 2023). To estimate cross-set thickness, flow depth, channel gradient, flow velocity, and unit water and sediment flux, rectangular (uniform) uncertainty distributions were used (see SM for extended methodology). This weights all uncertainty equally and avoids introduction of additional assumptions (cf. Lyster *et al.*, 2021). In channel width estimates, we employed triangular uncertainty distributions in some cases, as explained further below.

Cross-set Thickness

The primary palaeohydrological reconstruction available from cross-sets is the height of the original dune, h_d. This was estimated using the relation of Leclair & Bridge (2001) that mean cross-set thickness (h_xs) is, on average, around 1/3 of the original dune height:

$$h_\mathrm{d} = 2.9(\pm 0.7)h_\mathrm{xs}\,. \tag{1}$$

This formula is based on experimental data from rivers and flumes, and is rooted in the theoretical model developed by Paola & Borgman (1991) for dune migration over random topography on the bed with a low angle of climb, assuming the dunes are in equilibrium with the prevailing flow conditions. This model has been used to elucidate original dune height from stratigraphy in a range of geologic settings (Ganti *et al.*, 2019; Lyster *et al.*, 2021; McLeod *et al.*, 2023).

Flow Depth

Flow depth is an important metric in understanding the dynamics of ancient river systems. We used two approaches to estimate flow depth: a bedform approach, and a barform approach. The bedform approach uses the dataset of h_d in the relation of Bradley & Venditti (2017) to obtain an estimate of median flow depth, H:

$$H = xh_{\mathrm{d}}\,, \tag{2}$$

where x is a scalar based on a compilation of flow and dune dimension data. The relative heights of flow depth and dunes and cross-sets depends on flow stage (Das *et al.*, 2022), so uncertainty is represented in the scalar x which has an interquartile range between 4.4 and 10.1, and a median value of 6.7 (Bradley and Venditti, 2017). The results of this approach can be independently compared with barform data, using the thickness of bar accretion sets as robust architectural constraints on flow depth (Das *et al.*, 2022). These represent minimum bounds on bankfull flow depth, since barforms with measurable accretion surfaces have thickness equal to a minimum flow depth in formative conditions. Moreover, barform accretion packages are rarely fully preserved in fluvial strata, so reconstructed flow depths using the barform approach represent conservative minima. We do not consider compaction to have affected measured thickness of cross-sets or accretion sets, since it often has a relatively minor influence on sandstone-dominated units, and mostly when grain crushing occurs or when the initial sediment has anomalously high porosity or low proportions or cement (Fisher *et al.*, 1999).

Palaeoslope

Channel palaeoslope, S, was reconstructed using the approach of Trampush et al. (2014) based on empirical data rooted in hydrological theory, and is appropriate for the range of grain-sizes observed in the Montllobat and Castissent formations, including suspended, mixed and bedload rivers. S (in units of m/m) is given by:

$$logS = \alpha_0 + \alpha_1 logD_{50} + \alpha_2 logH\,, \tag{3}$$

where α_0, α_1 and α_2 are constants given as -2.08 ± 0.036, 0.254 ± 0.016 and -1.09 ± 0.044 respectively.

Flow Velocity and Unit Water Discharge

The formula established by Manning et al. (1890) was used to estimate water flow velocity, *U*:

$$U = \frac{1}{n} H^{\frac{2}{3}} S^{\frac{1}{2}}\,, \qquad (4)$$

where *n* is a roughness coefficient approximated as 0.03 (Lyster *et al.*, 2020). *U*, with units of m/s can be multiplied by flow depth to estimate the unit water discharge, q_w, in units of m^2/s: $q_w = UH$.

Sediment Flux

Reconstructing sediment flux through rivers is essential to understand their erosive and transport power: rates of sediment flux are highly sensitive to changing climate and tectonics (Sharma *et al.*, 2023; McLeod *et al.*, 2024; Prieur *et al.*, 2024; Rezwan *et al.*, 2025), and can inform about landscape dynamics from source to sink in the past. In this study, we tested several estimators of sediment flux, and base our results on the total load predictor of Engelund & Hansen (1967) for sand-dominated deposits and the bedload predictor of Meyer-Peter & Müller (1948) for gravel-dominated deposits. The relation of Engelund & Hansen (1967) gives sediment flux per unit width, q_s, in units of m^2/s width for sand-grade deposits as:

$$q_s = q_t^*(RgD_{50}^3)^{0.5}\,,$$

(5)

where *R* is the submerged density of sediment (~1.65 for quartz), g is 9.81 m/s^2 and D_{50} is the median grain-size. q^*_t is the non-dimensional Einstein number, relating shear stress and bed friction (see SM for extended methodology). For gravel-dominated channel deposits, we calculated unit bedload sediment flux using the formula of Meyer-Peter & Müller (1948) modified by Wong & Parker (2006):

$$Q_{s,bf} = \left(g\, D_{50}{}^{3}\, \Delta\rho\right)^{0.5} C(\tau_{*b} - \tau_{*c})^{\alpha}\,,$$

(6)

where Δρ is the dimensionless submerged specific gravity of sediment (1.6); dimensionless basal shear stress T^*_b is given as

$\tau_{*b} = H_{bf}S\ /\Delta\rho D_{50}$,

(7)

and dimensionless critical shear stress τ_{*c} and constants C and α are taken as 0.047, 4.93 and 1.6, respectively, after Wong & Parker (2006).

Channel Width

Estimating the width of active flow from stratigraphic deposits has been a continuing challenge in the field of fluvial geology. A range of evidence can be used to inform reconstructions of river width, including deposit lateral extent (e.g., Wood et al., 2022), numerous depth-scaling relations (e.g., Long, 2021), and barform accretion length (Greenberg *et al.*, 2021). Uncertainty in river width estimates is especially high when considering multi-threaded rivers. Estimates of width must be made in parallel with planform reconstructions to faithfully reconstruct ancient river morphology. Given previous work which interprets Montllobat and Castissent rivers as multi-threaded (Nijman & Nio, 1975; Van der Meulen, 1989), and results described below which support this, we used a formula for low-sinuosity rivers based on analysis by Long (2021) which relates bankfull width (W) to bankfull flow depth by:

$$W = 30.296H^{1.211}\ , \tag{15}$$

in a regression with an r^2 value of 0.61 and N = 990. This gives an estimate of the width of an individual channel (i.e. a single thread) based on values of H, and uncertainty is modelled using a rectangular distribution within the interquartile range of H. Rates of water and sediment discharge per channel, Q_w, (with units m^3/s) can be estimated according to $Q_w = q_w W$, where q_w is the discharge per unit width. To propagate uncertainty in channel width, we used a triangular distribution within the interquartile range, excluding outlying values that may represent river flow at extreme flow stages, which in multi-threaded rivers may alter active flow width significantly.

Planform

For total water and sediment discharge rates for the full river system, $Q_{s,w(total)}$, the number of threads in an ancient system must be estimated according to $Q_{total} = N_t Q$

where N_t is the number of active river threads or channels. We used two approaches to reconstruct the planform morphology of the Montllobat and Castissent rivers, described below.

Our first approach is based on dune-bar angular difference, Δ_{db}. The dominant bar mode in rivers is characteristic of planform morphology: lateral and upstream barform accretion is observed mainly in sinuous rivers, with single-threaded and meandering planform (e.g., (Miall, 1994; Rowley *et al.*, 2021). A dominantly downstream accreting bar mode is characteristic of low-sinuosity and braided rivers. In stratigraphy, dominant bar mode can be determined by calculating the angular difference between barform accretion orientation and the cross-set palaeoflow direction of dunes migrating over those bars. Where $\Delta_{db} < 35°$, the dominant bar mode is downstream accretion; where $35° \leq \Delta_{db} \geq 135°$, the dominant bar mode is lateral accretion; and where $\Delta_{db} > 135°$, the dominant bar mode is upstream accretion. We are able to check these results using dune cross-set palaeoflow circular variance, after Selley (1968), Le Roux (1992) and Galeazzi *et al.* (2021), explained further in the Supplemental Material.

Our second approach is based on work by Parker (1976) and Lyster et al. (2022). Parker (1976) theoretically derived planform stability fields, expressed as:

$$\varepsilon = \frac{S}{Fr}\frac{H}{W}\ , \tag{16}$$

where $\varepsilon < 1$ for single-threaded rivers, $\varepsilon > 1$ for multi-threaded rivers with 1–10 active channels, $\varepsilon > 10$ for multi-threaded rivers with more than 10 active channels, and Fr is the Froude number, calculated as

$$Fr = \frac{U}{\sqrt{gH}}\ . \tag{17}$$

Lyster et al. (2022) compiled a dataset of hydraulic geometries in natural rivers, and used these to update the stability fields for river planform geometries based on a much larger observational dataset. We estimate S, Fr, H and W for the rivers of the Montanyana Group and propagate uncertainty to generate a random distribution of 10^6 points within the range of uncertainty on a graph of S/Fr vs H/W to determine the likely planform morphology based on the stability fields of Lyster (2022).

RESULTS

Palaeohydrology Through Time

Through a comprehensive quantitative suite of palaeohydrologic techniques, we reconstruct the evolving morphodynamics of the Eocene Montllobat and Castissent Formations, and the rates and styles of water and sediment flow through these ancient river systems.

Based on full measured cross-set thickness distributions, the mean preserved cross-set thickness, h_{xs}, in the Montllobat fluvial sand bodies is 7.8 cm and 7.5 cm in the Castissent fluvial deposits. Our dataset describes cross-set thickness across the full down-system transects of c. 13 km in the Montllobat and c. 28 km in the Castissent, and there are no strong down-system trends in h_{xs} or grain-size (Supplemental Material). Therefore, we present results spatially averaged for each interval (the distribution of field data is presented on Fig. 1 and Fig. 3A). Using Equation 1 (Leclair & Bridge, 2001) we estimate that original dune height, h_d, averages 23 cm in the Montllobat and 22 cm in the Castissent. Two-tailed Kolmogorov-Smirov (K-S) tests unambiguously show that the full distributions of cross-sets from each formation are statistically different with 98.9% confidence, despite the medians being similar, while each member of the formations has cross-set thickness distributions which are statistically similar within each formation (Fig. 6A, bottom x-axis). This demonstrates that the Castissent and Montllobat formations have physically different properties to one-another at bedfom-scale.

The depth-scaling relation of Bradley & Venditti (2017) uses values of h_d to reconstruct median formative flow depths, H, of 1.36 m in the Montllobat Fm. and 1.26 m in the Castissent. Similarly to the original bedform data, the full distributions of reconstructed depths (Fig. 6A, top x-axis) are statistically different between the two formations, suggesting formative flow in the Castissent was marginally shallower.

Further constraints were made on flow depth based on a barform approach, using the heights of bar accretion sets. The median barform-derived flow depth is 1.40 m in both the Montllobat and the Castissent formations, with mean values of 1.42 m and 1.85 m, respectively. These results indicate that bedform- and barform-derived flow depth reconstructions are consistent, and confirm that assumptions of barform and bedform preservation inherent to the methods used are appropriate for these units.

Fluvial channels in the Montllobat Fm. are dominated by medium-grained sandstone, with an overall D_{50} of 0.38 mm. Castissent rivers had a bedload of coarse sand averaging 0.94 mm, however, both units contain some channelised, gravel-dominated conglomerates. Using estimates of H and D_{50}, we used Equation 3 (Trampush et al., 2014) to reconstruct palaeo-channel gradient, S. We find that Montllobat rivers had a median slope of 8.0×10^{-4} m/m (or 0.8 m/km) and Castissent rivers were 40% steeper with a median S value of 1.2×10^{-3} m/m. K-S tests on the full distribution of slope values (Fig. 6B), after Monte Carlo uncertainty propagation, demonstrate this increase in slope during the Castissent interval is statistically significant to 100.0% confidence.

These results show a clear change in palaeohydrological conditions between the two Formations, but analysis at Member level permits further temporal granularity in our analysis. Figure 7 illustrates changing H and S through the Montllobat and Castissent formations at Member-level, between 53.0 and 49.7 Ma. This reveals a steady shallowing in flow depth through time, coupled with a sharp increase in palaeoslope at the start of the Castissent interval, peaking in Castissent B.

Palaeohydraulic calculations also show that the unit water discharge and unit sediment discharge increase in the Castissent interval. Reconstructed H and S give median flow velocity, U, as 1.16 m/s in the Montllobat and 1.29 m/s in the Castissent. We then reconstruct q_w which averages 1.57 m^2/s in the Montllobat, and increases to 1.66 m^2/s by c. 50 Ma (Fig. 8A). Our sediment transport approach yields median unit sediment flux rates, q_s, of 3.6×10^{-3} m^2/s in the Montllobat and 2.6×10^{-3} m^2/s in the Castissent (Fig. 8B). Normalised per unit width and averaged per formation, water flux increases across the base of the Castissent, and sediment flux decreases. However, Member-level palaeohydrologic reconstructions (Figure 8B) reveal a consistent increase in unit sediment flux through the Castissent Formation. Median Formation-level unit water and sediment fluxes are skewed down by Castissent A which contains the majority of cross-set data, and is consistently most similar hydrologically to the Montllobat Formation. Note that these estimates do not consider the widths of river channel threads or of the total river channel belt.

Planform and Palaeoflow

Our first approach to reconstructing fluvial planform morphology is a dune-bar angular difference approach as this is routed in primary observational data. The median difference in orientation between preserved dune cross-set lee faces and barform accretion surfaces, Δ_{db}, in the Montllobat Fm. is 54°, 53° in MlbA and 59° in MlbB. In the Castissent Fm., the median Δ_{db} value is 38°, and in CstA, CstB and CstC the median Δ_{db} is 40°, 37° and 25° respectively

(Fig. 9A, Table 2). Downstream, lateral and upstream accreting bars are noted in multiple fluvial styles, but where a fluvial deposit dominantly preserves a certain bar mode, they can be used to interpret palaeo-planform. As illustrated in Figure 9A, this method of extracting bar modes from fluvial stratigraphy reveals a transition from more lateral-accretion-dominated planforms into a predominantly downstream-accretion-dominated planform over time, suggesting rivers became more braided in the Castissent interval. This is supported by low observed cross-set palaeoflow circular variance values, which are between 0.11 and 0.31 for the Montllobat (IQR) and 0.14 – 0.48 for the Castissent, with values as low as 0.04. This signature of low-variance dune migration is consistent with low-sinuosity multi-threaded river systems (Galeazzi *et al.*, 2021).

Our second approach, based on planform stability, ε (Parker, 1976; Lyster *et al.*, 2022a), requires estimates of river width. Using Eq. 15, we calculate channel width, W, from both barform and bedform approaches to reconstructing flow depth, which give similar results (Fig. 10). Using bedform-derived H estimates, individual river channels in the Montllobat Fm. had median widths of 44 m, and using barform-derived H values, channels averaged 45 m wide. For the Castissent Fm., the median bedform-derived W estimate is 40 m, and using the barform approach, channels could have been 46 m wide. In further analysis, we favour the barform-derived estimates of channel width, as they represent more robust architectural constraints on channel morphology and introduce fewer uncertainties.

We model the number of active channel threads, N_t, using a rectangular distribution of values within the range of uncertainty. To estimate a maximum N_t, we used the average width of amalgamated multi-lateral sandstone bodies observed. In the Castissent Fm., sandstone bodies average 1.0 km wide, and the average is 0.5-0.6 km in the Montllobat Fm. These represent conservative lower limits on the width of the alluvial plain, and an upper limit on the width of active flow. Therefore, we use these values along with estimates of W, above, to calculate the likely maximum number of channel threads. This is $N_t = 7$ in the Montllobat and $N_T = 11$ in the Castissent. We set the lower limit for N_T as 1 in the Montllobat and 2 in the Castissent, given we and others (Cabello *et al.*, 2018) identify single-threaded reaches in the Montllobat, but interpret the Castissent as braided, with no single-threaded reaches (see SM for full uncertainty distributions). These yield median total active flow widths, W_{total}, of 205 and 225 m in the Montllobat and Castissent Formations, respectively. Using estimates of W_{total}, Fr, H and U (Eq. 16), planform geometry can be compared to stability fields generated based on theory and observations of modern and ancient rivers (Parker, 1976; Lyster *et al.*, 2022a). Figure 9C shows that according to the dataset of Lyster (2022), the typical median Castissent river was stable in a braided planform. This approach suggests Montllobat rivers had some single-threaded reaches but were broadly stable with an anastomosing planform, defined by Lyster (2022) as $S/Fr > 0.003$ and $H/W < 0.2$. Makaske (2001) defines anastomosing rivers as composed of two or more interconnected channels that enclose floodbasins. This interpretation is supported by facies observations, including those of (Cabello *et al.*, 2018).

To summarise, recovered bar modes and planform stability analysis shows that what started as anastomosing rivers with some single-threaded reaches transitioned into braided systems by the time of the Castissent interval.

Total Fluxes

The above palaeohydraulic reconstructions of unit discharges and unit sediment fluxes explicitly do not include channel width, which is the most challenging aspect of this type of stratigraphic reconstruction (Long, 2021). However, combining unit fluxes with river planform estimates and thread width estimates (Figures 9 and 10), we can investigate foreland-scale geomorphology in the early Pyrenees by estimating total water and sediment loads to first order, as represented in the Montanyana Group.

Total active flow widths are estimated to average 205 and 225 m respectively for the Montllobat and Castissent Formations. Since total discharge is a product of unit discharge and total active flow width, we use our results to reconstruct a median estimate of $Q_{w(total)}$ in the Montllobat Fm. of ca. 280 m^3/s, and ca. 420 m^3/s in the Castissent, a 40% increase. For total sediment discharge, $Q_{s(total)}$ increased from 0.6 m^3/s in the Montllobat to 0.7 m^3/s in the Castissent, a 10-15% difference at median level. Whilst this change in sediment flux appears modest, Figure 11 depicts graphically the changing total fluxes and uncertainty through time, and highlights a consistent increase in sediment load through time. These estimates quantitatively describe material flux through the rivers of the Eocene Hothouse, and how they behaved in space and time. But how unique are these river deposits geologically, and what environmental and tectonic forcings contributed to the hydrology of the Montanyana Group?

DISCUSSION

Modern Analogues

Using a suite of quantitative palaeohydrologic techniques based on geologic field data, we reveal the lower Eocene rivers of the Montanyana Group became increasingly multi-threaded through time, were on average 1.2 – 1.4 m deep (but could be deeper than 5 m, based on maximum barform accretion set thicknesses), with channel slopes of 0.5 – 0.7°. We show a marked increase in river slope and discharge 50.5 Mya, and a shift in planform coinciding with the onset of Castissent progradation and an increase in sediment flux, supporting and furthering the findings of previous qualitative investigations. This represents the most robust quantitative description of Ypresian rivers in the Pyrenees to date. But how do these rivers compare to modern examples, given they were deposited during a period of marked global warmth compared to today?

We compare results to a global database of modern river morphology and hydrology (Lyster *et al.*, 2022a). We find that there are no identical modern analogues for the Montllobat and Castissent systems. Considering similarity in planform, discharge, width, slope and grain-size, they might have looked similar to the Tanana and Saskatchewan rivers, Alaska; Athabasca river, Canada; Wairau river, New Zealand; Durack river, northwestern Australia; or the Yuma Wash river, Arizona. However, on average, reconstructed *W/H* ratio was lower in the Montanyana Group than in most modern sand-bedded multi-threaded rivers with similar water discharge rates. Moreover, modern multi-threaded sand-bedded rivers have flow velocity averaging 1.0 m/s, slower than those in the lower Eocene Pyrenean foreland. This suggests either a bias in our results related to preservation of small rivers, or suggesting Montanyana rivers were somewhat deeper and faster than modern analogues with similar planform.

Furthermore, geochemical data acquired from Castissent floodplain deposits show the environment of the early Eocene was semi-arid to sub-humid with seasonal humidity patterns (Honegger *et al.*, 2020). Today, no braided, sand-bed rivers with similar water discharge rates are observed in regions with seasonally subhumid climate (Beck *et al.*, 2018). Considering these constraints, the most likely modern analogues for the Castissent Fm. are the braided Gangetic rivers of the Himalayan foreland, with comparable fluvial morphology, climate characteristics and tectonic setting to that in the lower Eocene, albeit with much larger catchments and discharge rates (Lyster *et al.*, 2022a). Their flow velocity, aspect ratio, planform and bedload grain-size, all in a small orogenic setting and sub-arid climate make Montanyana rivers unique compared to rivers today. What antecedent conditions permitted this, and how do these ancient systems compare to others recorded in stratigraphy?

Climate or tectonics?

Disentangling climatic from tectonic signals in the fluvial archive is an ongoing research challenge: our results show clear signatures of both. The Castissent rivers were on average twice as coarse in their bedload, 1.4 times as steep, had 40% more water discharge and 10-15% more sediment discharge, and were more strongly braided in comparison to the underlying Montllobat Fm. Notably, the ratio of Q_s to Q_w (the sediment flux intensity) is 46% lower in the Castissent, meaning it transported more water per unit sediment discharge than the Montllobat. These changes point to a clear climatic driver.

There are a growing number of stratigraphic case studies documenting changing material flux in the geologic record due to climate change. For example, the Palaeocene-Eocene Thermal Maximum (PETM) is recorded in fluvial successions of the southern Pyrenees, where a two-fold increase in Q_s is observed in the Claret Conglomerate (Prieur et al., in review), associated with a 3-8°C increase in mean annual temperature (MAT), a 27% increase in mean annual precipitation (MAP) and high rates of channel amalgamation. Additionally, the upper Eocene Escanilla Fm. (S. Pyrenees) spanning the Mid Eocene Climate Optimum (MECO) records a 50% increase in Q_s and S in intervals with highly amalgamated sandbodies, compared to low-amalgamation intervals (Sharma *et al.*, 2023). These are interpreted to have been caused by climate-driven water discharge variation, with a three-fold increase in Q_w. Moreover, sediment transport is projected to increase in modern river systems due to current global warming (McLeod *et al.*, 2024). So changing sediment flux is a documented result of climate change in geomorphic systems in the past and present, and is usually associated with increased amalgamation of channel-fill sand and conglomerate bodies.

However, despite a clear hydrologic shift at the onset of the Castissent Fm., this interval is not associated with a climate signal lasting 800 kyrs. On the contrary, Castissent deposition is associated with both a gradual reduction in global temperatures at the end of the EECO (Fig. 2), and superimposed hyperthermal events, which, together with a potential tectonic signal, combined to cause 20 km of progradation.

Progradation is well-documented in the Castissent in a stratigraphic context (e.g. Marzo et al., 1988), and is observed here in an increase in slope and D_{50} from the Montllobat into the Castissent (averaged across the total dip-section), demonstrating a down-system shift in fluvial facies. It has been hypothesised that Castissent progradation could be due to an Ypresian sea-level fall, reducing accommodation space and increasing amalgamation (Marzo *et al.*, 1988; Whitchurch *et al.*, 2011; Honegger *et al.*, 2020). However, in this hothouse climate there was no glacial eustatic sea-level change, with no Antarctic ice sheet until c. 34 Mya (Hutchinson *et al.*, 2021), so some other mechanism of significant sea-level change would be required. Some authors (e.g., Sames et al., 2020) have suggested aquifer eustasy can be a dominant cause of sea-level change in hothouse climates, whereas others find this process is capable only of decimetre-scale sea-level change (Davies *et al.*, 2020). Notwithstanding its cause, regression cannot explain the increase in total water flux, which requires a climatic driver.

It is possible, on the other hand, that progradation and steepening was tectonically derived. Thermochronologic modelling (Whitchurch *et al.*, 2011) suggests there was a pulse of tectonic uplift observed across the southern Pyrenees focused at c. 50.9 Ma, and Curry et al.'s (2021) findings suggest Castissent progradation c. 50 Ma could be related to a 2.4-fold increase in exhumation rate in the Castissent's likely headwater region (Fig. 2B). This presents a strong argument for a tectonic-driven geomorphic change in the Castissent, but changing exhumation rates could be tied equally to tectonic uplift or to climate-driven erosion and denudation. The timing of this rate change is also poorly constrained due to the temporal distribution of thermochronologic data points in the Castissent's headwater region.

Nonetheless, while the observed increase in slope, grain-size and sediment could be explained by an increase in uplift rate, we know that tectonics cannot be the only contributor: firstly, we interpret a 40% increase in water discharge, Q_w. Whilst this could be tectonically-driven due to an increase in catchment size, we do not believe this is the primary cause of the increase in discharge. A switch to a heightened uplift rate for a prolonged period in the hinterland catchments of this system, as modelled by Curry et al. (2021, Fig. 2), should in theory lead to a permanent increase in sediment flux as topographic steady state is re-achieved (Armitage *et al.*, 2011). On the contrary, the Castissent Formation records 800 kyrs of heightened water and sediment flux, followed by the Upper Montanyana Group and a return to a similar depositional character and facies distribution (Fig. 3) to that of the underlying Montllobat Fm (Nijman & Nio, 1975; Marzo *et al.*, 1988; Nijman, 1998). Consequently, the stratigraphic architecture and facies distributions of the Montanyana Group (Fig. 3) imply an increase in sediment flux that was transient (Nijman, 1998; Armitage *et al.*, 2011), unlike the regional tectonic trends, suggesting a climate is a likely contributer. This return to similar facies distributions in the

Upper Montanyana Group also makes tectonically-induced catchment widening an unlikely cause for the change in hydrology in the Castissent.

After the PETM, the Ypresian climate is characterised by a broad warming trend climaxing in the EECO, before a gradual cooling and levelling off by 50 Ma (Fig. 2, Westerhold et al., 2018). Honegger et al. (2020) interpret semi-arid to sub-humid average climates in the Castissent interval based on CaO/Al_2O_3 ratios in floodplain sediment, and seasonal humidity patterns based on the smectite/kaolinite ratio in palaeosols and the presence of nodules composed of concentric haematite and goethite found together with carbonate nodules. In the Montllobat on the other hand, humidity and precipitation rates are not well-constrained, so we cannot directly interpret a clear change in humidity at the onset of the Castissent.

The Castissent interval contains three hyperthermals recognised in $\delta^{13}C$ records of benthic carbonates (Westerhold *et al.*, 2017; Honegger *et al.*, 2020). Hyperthemal "S" coincides with the onset of Castissent sedimentation, followed shortly by hyperthermal "T," but Honegger et al. (2020) identify only the geochemical signature of the subsequent hyperthermal "U" recorded in the floodplain above Castissent A in the Chiriveta section (Fig. 1, 2). It is dated to 50.0 Ma and is associated with a MAT increase of 2 - 3°C that could have had a duration as short as 40 kyrs, but preserves a signal climax lasting 150 kyrs (c. 50.10 – 49.95 Ma) in stratigraphy – the duration likely augmented by the dynamic nature of fluvial deposition. Significantly, we do not see a uniform signal across the Castissent Formation, but Castissent B which was likely deposited during c. 50.0 – 49.8 Ma preserves the most significant signal of enhanced S and Q_w, followed by Q_s peaking in CstC (Fig. 8). The onset of the Castissent could be related to hyperthermals "S" and "T" (Fig. 2A). Subsequently, the prolonged signal of hyperthermal "U", representing the delayed fluvial response to a negative $\delta^{13}C$ excursion, could be manifest in the rock record in the geomorphology of Castissent B followed by a disequilibrium enhancement in sediment flux in Castissent C. The strong change in formative discharge conditions observed at both channel and braidplain scale in the absence of large changes in yearly rainfall typically relates to the distribution and magnitude of individual storm or monsoon events (Molnar *et al.*, 2006).

Palaeobotanial proxies (Greenwood & Huber, 2011) suggest that throughout the early-mid Eocene, Earth's climate was controlled by a global monsoon cycle, driving strongly seasonal precipitation patterns. It has also been observed that temperature increase causes enhanced monsoon cycles (Loo *et al.*, 2015), and has caused increased humidity and precipitation in the

PETM of the Pyrenees (Prieur *et al.*, 2024). Does palaeohydrology support this hypothesis, and could the three global CIE hyperthermals between 50.5 and 49.7 Ma have affected monsoon cycles and caused the stratigraphic marker of the Castissent Formation?

Hydrological calculations suggest discharge in the Montanyana rivers was variable enough to suggest monsoonal rainfall patterns: if we model the MAP of 376 mm/a (Honegger *et al.*, 2020) to rain on an estimated Castissent catchment of c. 10,000 km^2 – based on compiled palaeogeographic reconstructions and independent constraints on altimetry and sediment routing (Huyghe *et al.*, 2012; Curry *et al.*, 2019; Markwick, 2019; Juvany *et al.*, 2024) – this implies mean flow of under 1/3 the discharge of channel-forming conditions reconstructed here. From this we could estimate a monsoon precipitation index (MPI, Wang & Ding, 2008), i.e., the ratio between the annual precipitation range and the MAP. We assume here this is equivalent to the difference between the bankfull and mean annual discharge (MAD), divided by the MAD. This calculation yields a value of 2.5, suggesting strongly variable rainfall that could be driven by the monsoon cycles observed by (Greenwood & Huber, 2011). This supports the geochemical findings of Honegger et al. (2020) that the climate was highly seasonal. Plink-Bjorklund (2015) compiled a series of facies indicators for monsoon-dominated fluvial systems in the rock record. These types of rivers are often dominated by downstream accreting bars and an absence of well-preserved lateral accretion, and these indicators are increasingly dominant up-section (Fig. 9A). However, monsoonal systems are also expected to record dominant soft sediment deformation, fossilised in-channel vegetation and upper-flow regime sedimentary structures (Plink-Bjorklund, 2015) – we observe these rarely in the Montanyana Group.

Therefore, we hypothesise that the levelling-off in global cooling at the end of the EECO followed by three hyperthermal events may have driven changes to the global monsoon cycle and this affected discharge rates in the Pyrenees. There is also precedent for change to monsoon cycles on similar timescales driven by climate: modern climate change in combination with the uplift of the Himalayan plateau has enhanced the Indian summer monsoon (ISM) and altered river hydrology in the present-day Himalayan foreland (Loo *et al.*, 2015). In the same setting at 4.2ka, δ18O records, fluvial sedimentology and other proxies from Holocene sediments in the Indus Valley (Giosan *et al.*, 2012; Dixit *et al.*, 2014; Dutt *et al.*, 2018) show a weakening of the ISM caused by abrupt cooling. This significantly reduced Indus river discharge, contributing to the decline of the Harappan civilisation (Giosan *et al.*, 2012). So it seems possible that climate change caused the shift in monsoon discharge and river activity in the

Montanyana rivers on a short timescale. Perhaps the modern Himalaya are a strong analogue for the evolving Montanyana rivers – with a similar tectono-climatic setting and with abrupt increases in temperature and humidity strengthening monsoon cycles and affecting hydrology.

Comparing the global $\delta^{13}C$ record with exhumation profiles for the Ypresian Pyrenees (Fig. 2) establishes that the observed morphological and hydrodynamic shift observed at 50.5 Ma occurs at the superimposition of a gradual global cooling, an increase in hinterland exhumation rate, and the occurrence of three transient hyperthermal events. We hypothesise the anastomosing Montllobat rivers from 53 – 50.5 Ma responded to a gradually cooling climate with intermittent flow, and a bedload of medium sand was transported as a large proportion of its water discharge, explaining observed Q_s/Q_w ratios. Conversely, the overlying Castissent saw cooling level off, an increase in tectonic uplift rate, and an enhanced global monsoon driven by hyperthermal events. Triggered by this, Montanyana rivers became temporarily steeper, faster, and more strongly braided, with more sustained water discharge and transport of coarse sediment from the growing Pyrenees lasting 800 kyrs, and resulting in a 20 km progradation of fluvial facies.

The remaining unknown concerns the role of the patterns of climate-driven precipitation in driving fluvial geomorphic change in the Montanyana Group, and the importance of hyperthermal events in controlling river sedimentation in monsoonal systems. In order to quantitatively disentangle climate change from the tectonic signal of the growing Pyrenees, mean conditions are not enough. The frequency and patterns of threshold-surpassing events – river intermittency – could be what controls transient landscape response to climate drivers (McLeod *et al.*, 2024). Combined with this study's quantification of landscape-scale fluvial geomorphology, this next step could complete the picture of landscape dynamics in the Montanyana Group.

CONCLUSIONS

The lower Eocene Montllobat and Castissent Formations of the southern Pyrenees record a geomorphic event towards the end of the EECO which saw coarse-grained fluvial sandstones prograde 20 km seaward within an 800 ka period. Using a quantitative field-based palaeohydrologic framework across 4 field sites, we establish strong constraints on the evolving hydrodynamics of these ancient river systems. We show that the start of the Castissent interval at c. 50.5 Ma is associated with a statistically significant reduction in cross-set thickness, a doubling of the median grain-size and a 1.4-fold increase in channel slope. We reconstruct a 40% increase in total water discharge from the Montllobat to the Castissent Formation, a 15% increase in sediment discharge, and a signature of sustained precipitation. We also quantify a shift in fluvial planform morphology: Castissent rivers exhibited more pronounced braiding than the mostly anastomosing Montllobat Formation before it, and we track these trends through time, showing a sharp change in hydrodynamics. These results, in combination with climate and exhumation records for the southern Pyrenees, suggest that the Castissent Formation represents the transient product of multiple climatic signals within the context of an evolving mountain range: a levelling off in a long-term cooling trend at the end of the EECO, three superimposed hyperthermal events, and an increase in tectonic uplift rate at c. 50.5 Mya. We hypothesise this climate change caused enhanced monsoon precipitation and more sustained river discharge, driving a significant shift in fluvial hydrodynamics and geomorphology. This analysis sheds light on river dynamics in an environment analogous to a future climate scenario, and reveals the potential in quantitative palaeohydrology to extract complex tectono-climatic signals from stratigraphy. Further investigation into the patterns of water and sediment transport through the lower Eocene could help determine the extent to which climate change can cause significant shifts in fluvial activity and landscape dynamics.

ACKNOWLEDGEMENTS

This work was supported by the Natural Environment Research Council (grant NE/S007415/1) and Terrabotics (London). MATLAB (MathWorks) was used in our analyses.

BIBLIOGRAPHY

Allmendinger, R.W., **C., C., N.** and **Fisher, D.** (2013) Structural Geology Algorithms: Vectors & Tensors.

Armitage, J.J., **Duller, R.A.**, **Whittaker, A.C.** and **Allen, P.A.** (2011) Transformation of tectonic and climatic signals from source to sedimentary archive. *Nature Geosci*, **4**, 231–235.

Beck, H.E., **Zimmermann, N.E.**, **McVicar, T.R.**, **Vergopolan, N.**, **Berg, A.** and **Wood, E.F.** (2018) Present and future Köppen-Geiger climate classification maps at 1-km resolution. *Sci Data*, **5**, 180214.

Bradley, R.W. and **Venditti, J.G.** (2017) Reevaluating dune scaling relations. *Earth-Science Reviews*, **165**, 356–376.

Cabello, P., **Domínguez, D.**, **Murillo-López, M.H.**, **López-Blanco, M.**, **García-Sellés, D.**, **Cuevas, J.L.**, **Marzo, M.** and **Arbués, P.** (2018) From conventional outcrop datasets and digital outcrop models to flow simulation in the Pont de Montanyana point-bar deposits (Ypresian, Southern Pyrenees). *Marine and Petroleum Geology*, **94**, 19–42.

Caja, M.A., **Marfil, R.**, **Garcia, D.**, **Remacha, E.**, **Morad, S.**, **Mansurbeg, H.**, **Amorosi, A.**, **Martínez-Calvo, C.** and **Lahoz-Beltrá, R.** (2010) Provenance of siliciclastic and hybrid turbiditic arenites of the Eocene Hecho Group, Spanish Pyrenees: implications for the tectonic evolution of a foreland basin. *Basin Research*, **22**, 157–180.

Chanvry, E., **Deschamps, R.**, **Joseph, P.**, **Puigdefàbregas, C.**, **Poyatos-Moré, M.**, **Serra-Kiel, J.**, **Garcia, D.** and **Teinturier, S.** (2018) The influence of intrabasinal tectonics in the stratigraphic evolution of piggyback basin fills: Towards a model from the Tremp-Graus-Ainsa Basin (South-Pyrenean Zone, Spain). *Sedimentary Geology*, **377**, 34–62.

Clark, J.D. and **Pickering, K.T.** (1996) Architectural Elements and Growth Patterns of Submarine Channels: Application to Hydrocarbon Exploration1. *AAPG Bulletin*, **80**, 194–220.

Cornard, P. and **Pickering, K.** (2020) Submarine topographic control on distribution of supercritical-flow deposits in lobe and related environments, middle Eocene, Jaca Basin, Spanish Pyrenees. *Journal Of Sedimentary Research*, 1222–1243.

Curry, M.E., **Beek, P.V.D.**, **Huismans, R.S.**, **Wolf, S.G.**, **Fillon, C.** and **Muñoz, J.-A.** (2021) Spatio-temporal patterns of Pyrenean exhumation revealed by inverse thermo-kinematic modeling of a large thermochronologic data set. *Geology*, **49**, 738–742.

Curry, M.E., **van der Beek, P.**, **Huismans, R.S.**, **Wolf, S.G.** and **Muñoz, J.-A.** (2019) Evolving palaeotopography and lithospheric flexure of the Pyrenean Orogen from 3D flexural modeling and basin analysis. *Earth and Planetary Science Letters*, **515**, 26–37.

Das, D., **Ganti, V.**, **Bradley, R.**, **Venditti, J.**, **Reesink, A.** and **Parsons, D.R.** (2022) The Influence of Transport Stage on Preserved Fluvial Cross Strata. *Geophysical Research Letters*, **49**, e2022GL099808.

Davies, A., **Gréselle, B.**, **Hunter, S.J.**, **Baines, G.**, **Robson, C.**, **Haywood, A.M.**, **Ray, D.C.**, **Simmons, M.D.** and **van Buchem, F.S.P.** (2020) Assessing the impact of aquifer-eustasy on short-term Cretaceous sea-level. *Cretaceous Research*, **112**, 104445.

Dixit, Y., **Hodell, D.A.** and **Petrie, C.A.** (2014) Abrupt weakening of the summer monsoon in northwest India ~4100 yr ago. *Geology*, **42**, 339–342.

Dutt, S., **Gupta, A.K.**, **Wünnemann, B.** and **Yan, D.** (2018) A long arid interlude in the Indian summer monsoon during ∼4,350 to 3,450 cal. yr BP contemporaneous to displacement of the Indus valley civilization. *Quaternary International*, **482**, 83–92.

Emiliano Mutti and **Maria Sgavetti** (1987) Sequence stratigraphy of the upper cretaceous aren strata in the orcau-aren region, south-central pyrenees, spain: distinction between eustatically and tectonically controlled depositional sequences. *Annali Dell'Universita di Ferrara Sezione Scienze Della Terra*, **1**, 1–21.

Engelund, F. and **Hansen, E.** (1967) A monograph on sediment transport in alluvial streams.

Fielding, C.R., **Alexander, J.** and **Allen, J.P.** (2018) The role of discharge variability in the formation and preservation of alluvial sediment bodies. *Sedimentary Geology*, **365**, 1–20.

Fisher, Q.J., **Casey, M.**, **Clennell, M.B.** and **Knipe, R.J.** (1999) Mechanical compaction of deeply buried sandstones of the North Sea. *Marine and Petroleum Geology*, **16**, 605–618.

Flannigan, M.D., **Amiro, B.D.**, **Logan, K.A.**, **Stocks, B.J.** and **Wotton, B.M.** (2006) Forest Fires and Climate Change in the 21ST Century. *Mitig Adapt Strat Glob Change*, **11**, 847–859.

Galeazzi, C.P., **Almeida, R.P.** and **do Prado, A.H.** (2021) Linking rivers to the rock record: Channel patterns and palaeocurrent circular variance. *Geology*, **49**, 1402–1407.

Ganti, V., **Whittaker, A.C.**, **Lamb, M.P.** and **Fischer, W.W.** (2019) Low-gradient, single-threaded rivers prior to greening of the continents. *Proceedings of the National Academy of Sciences*, **116**, 11652–11657.

Gariano, S.L. and **Guzzetti, F.** (2016) Landslides in a changing climate. *Earth-Science Reviews*, **162**, 227–252.

Giosan, L., **Clift, P.D.**, **Macklin, M.G.**, **Fuller, D.Q.**, **Constantinescu, S.**, **Durcan, J.A.**, **Stevens, T.**, **Duller, G.A.T.**, **Tabrez, A.R.**, **Gangal, K.**, **Adhikari, R.**, **Alizai, A.**, **Filip, F.**, **VanLaningham, S.** and **Syvitski, J.P.M.** (2012) Fluvial landscapes of the Harappan civilization. *Proceedings of the National Academy of Sciences*, **109**, E1688–E1694.

Greenberg, E., **Ganti, V.** and **Hajek, E.** (2021) Quantifying bankfull flow width using preserved bar clinoforms from fluvial strata. *Geology*, **49**, 1038–1043.

Greenwood, D.R. and **Huber, M.** (2011) Eocene precipitation: a global monsoon? **2011**, T22C-07.

Honegger, L., **Adatte, T.**, **Spangenberg, J.E.**, **Rugenstein, J.K.C.**, **Poyatos-Moré, M.**, **Puigdefàbregas, C.**, **Chanvry, E.**, **Clark, J.**, **Fildani, A.**, **Verrechia, E.**, **Kouzmanov, K.**, **Harlaux, M.** and **Castelltort, S.** (2020) Alluvial record of an early Eocene hyperthermal within the Castissent Formation, the Pyrenees, Spain. *Clim. Past*, **16**, 227–243.

Hutchinson, D.K., **Coxall, H.K.**, **Lunt, D.J.**, **Steinthorsdottir, M.**, **de Boer, A.M.**, **Baatsen, M.**, **von der Heydt, A.**, **Huber, M.**, **Kennedy-Asser, A.T.**, **Kunzmann, L.**, **Ladant, J.-B.**, **Lear, C.H.**, **Moraweck, K.**, **Pearson, P.N.**, **Piga, E.**, **Pound, M.J.**, **Salzmann, U.**, **Scher, H.D.**, **Sijp, W.P.**, **Śliwińska, K.K.**, **Wilson, P.A.** and **Zhang, Z.** (2021) The Eocene–Oligocene transition: a review of marine and terrestrial proxy data, models and model–data comparisons. *Climate of the Past*, **17**, 269–315.

Huyghe, D., **Mouthereau, F.** and **Emmanuel, L.** (2012) Oxygen isotopes of marine mollusc shells record Eocene elevation change in the Pyrenees. *Earth and Planetary Science Letters*, **345–348**, 131–141.

IPCC (2022) IPCC, 2022: Climate Change 2022: Impacts, Adaptation, and Vulnerability. Contribution of Working Group II to the Sixth Assessment Report of the Intergovernmental Panel on Climate Change. *Cambridge University Press, Cambridge, UK and New York, NY, USA*.

Jaimes-Gutierrez, R., **Adatte, T.**, **Pucéat, E.**, **Vennemann, T.**, **Prieur, M.**, **Wild, A.L.**, **Khozyem, H.**, **Vaucher, R.** and **Castelltort, S.** (2024) Deciphering Palaeocene-Eocene Thermal Maximum Climatic Dynamics: Insights From Oxygen and Hydrogen Isotopes in Clay Minerals of Palaeosols From the Southern Pyrenees. *Palaeoceanography and Palaeoclimatology*, **39**, e2024PA004858.

Juvany, P., **Garcés, M.**, **López-Blanco, M.**, **Valero, L.**, **Amorós, E.B.**, **Poyatos-Moré, M.** and **Rius, A.M.** (2024) Unraveling the sediment routing systems evolution of the south Pyrenean foreland basin during the lower to middle Palaeogene period. *Marine and Petroleum Geology*, **167**, 106913.

Le Roux, J.P. (1992) Determining the channel sinuosity of ancient fluvial systems from palaeocurrent data. *Journal of Sedimentary Research*, **62**, 283–291.

Leclair, S. and **Bridge, J.** (2001) Quantitative Interpretation of Sedimentary Structures Formed by River Dunes. *Journal of Sedimentary Research - J SEDIMENT RES*, **71**, 713–716.

Long, D.G.F. (2021) Trickling down the palaeoslope: an empirical approach to palaeohydrology. *Earth-Science Reviews*, **220**, 103740.

Loo, Y.Y., **Billa, L.** and **Singh, A.** (2015) Effect of climate change on seasonal monsoon in Asia and its impact on the variability of monsoon rainfall in Southeast Asia. *Geoscience Frontiers*, **6**, 817–823.

Lyster, S.J. (2022) Quantifying the dynamics and behaviour of ancient fluvial systems in space and time. Imperial College London

Lyster, S.J., **Whittaker, A.C.**, **Allison, P.A.**, **Lunt, D.J.** and **Farnsworth, A.** (2020) Predicting sediment discharges and erosion rates in deep time—examples from the late Cretaceous North American continent. *Basin Research*, **32**, 1547–1573.

Lyster, S.J., **Whittaker, A.C.** and **Hajek, E.A.** (2022a) The problem of palaeo-planforms. *Geology*, **50**, 822–826.

Lyster, S.J., **Whittaker, A.C.**, **Hajek, E.A.** and **Ganti, V.** (2022b) Field evidence for disequilibrium dynamics in preserved fluvial cross-strata: A record of discharge variability or morphodynamic hierarchy? *Earth and Planetary Science Letters*, **579**, 117355.

Lyster, S.J., **Whittaker, A.C.**, **Hampson, G.J.**, **Hajek, E.A.**, **Allison, P.A.** and **Lathrop, B.A.** (2021) Reconstructing the morphologies and hydrodynamics of ancient rivers from source to sink: Cretaceous Western Interior Basin, Utah, USA. *Sedimentology*, **68**, 2854–2886.

Makaske, B. (2001) Anastomosing rivers: a review of their classification, origin and sedimentary products. *Earth-Science Reviews*, **53**, 149–196.

Manning, R., **Griffith, J.P.**, **Pigot, T.F.** and **Vernon-Harcourt, L.F.** (1890) On the flow of water in open channels and pipes. 161 pp.

Markwick, P.J. (2019) Palaeogeography in exploration. *Geol. Mag.*, **156**, 366–407.

Marzo, M., **Nijman, W.** and **Puigdefabregas, C.** (1988) Architecture of the Castissent fluvial sheet sandstones, Eocene, South Pyrenees, Spain. *Sedimentology*, **35**, 719–738.

McInerney, F. and **Wing, S.** (2011) The Palaeocene-Eocene Thermal Maximum: A Perturbation of Carbon Cycle, Climate, and Biosphere with Implications for the Future. *Annu. Rev. Earth Planet. Sci.*, **39**, 489–516.

McLeod, J.S., **Whittaker, A.C.**, **Bell, R.E.**, **Hampson, G.J.**, **Watkins, S.E.**, **Brooke, S.A.S.**, **Rezwan, N.**, **Hook, J.**, **Zondervan, J.R.**, **Ganti, V.** and **Lyster, S.J.** (2024) Landscapes on the edge: River intermittency in a warming world. *Geology*, **52**, 512–516.

McLeod, J.S., **Wood, J.**, **Lyster, S.J.**, **Valenza, J.M.**, **Spencer, A.R.T.** and **Whittaker, A.C.** (2023) Quantitative constraints on flood variability in the rock record. *Nat Commun*, **14**, 3362.

Meyer-Peter, E. and **Müller, R.** (1948) Formulas for Bed-Load transport.

Miall, A.D. (1994) Reconstructing fluvial macroform architecture from two-dimensional outcrops; examples from the Castlegate Sandstone, Book Cliffs, Utah. *Journal of Sedimentary Research*, **64**, 146–158.

Milliman, J.D. and **Meade, R.H.** (1983) World-Wide Delivery of River Sediment to the Oceans. *The Journal of Geology*, **91**, 1–21.

Molnar, P., **Anderson, R.S.**, **Kier, G.** and **Rose, J.** (2006) Relationships among probability distributions of stream discharges in floods, climate, bed load transport, and river incision. Journal of Geophysical Research: Earth Surface. doi: 10.1029/2005JF000310

Nijman, W. (1998) Cyclicity and basin axis shift in a piggyback basin: towards modelling of the Eocene Tremp-Ager Basin, South Pyrenees, Spain. *SP*, **134**, 135–162.

Nijman, W. and **Nio, S.D.** (1975) The Eocene Montañana Delta: Tremp-Graus Basin, Provinces of Lérida and Huesca, Southern Pyrenees, N. Spain). *Vakgroep Sedimentologie, Rijksuniveriteit Leiden-Utrecht*, 20 pp.

Nijman, W. and **Puigdefàbregas, C.** (1977) Coarse-Grained Point Bar Structure in a Molasse-Type Fluvial System, Eocene Castisent Sandstone Formation, South Pyrenean Basin.

Paola, C. and **Borgman, L.** (1991) Reconstructing random topography from preserved stratification. *Sedimentology*, **38**, 553–565.

Parker, G. (1976) On the cause and characteristic scales of meandering and braiding in rivers. *Journal of Fluid Mechanics*, **76**, 457–480.

Picart, J., **Samso, J.**, **Cuevas, J.L.**, **Mercade, L.** and **Arbues, P.** (2010) Mapa Geologic de Catalunya 1:2500. Espills 251-2-2 (64-22).

Plink-Bjorklund, P. (2015) Morphodynamics of rivers strongly affected by monsoon precipitation: Review of depositional style and forcing factors. Sedimentary Geology. doi: 10.1016/j.sedgeo.2015.04.004

Prieur, M., **Robin, C.**, **Braun, J.**, **Vaucher, R.**, **Whittaker, A.**, **Jaimes Gutiérrez, R.**, **Wild, A.**, **McLeod, J.**, **Malatesta, L.**, **Fillon, C.**, **Schlunegger, F.**, **Sømme, T.** and **Castelltort, S.** (2024) Climate Control on Erosion: Evolution of Sediment Flux from Mountainous Catchments during a Global Warming Event, PETM, Southern Pyrenees, Spain.

Puig, J.M., **Cabello, P.**, **Howell, J.** and **Arbués, P.** (2019) Three-dimensional characterisation of sedimentary heterogeneity and its impact on subsurface flow behaviour through the braided-to-meandering fluvial deposits of the Castissent Formation (late Ypresian, Tremp-Graus Basin, Spain). *Marine and Petroleum Geology*, **103**, 661–680.

Rezwan, N., **Whittaker, A.C.**, **McLeod, J.S.**, **Hook, J.**, **Castelltort, S.** and **Schlunegger, F.** (2025) Decoding Normal-Fault Controlled Trends in Stratigraphic Grain Size: Examples From the Kerinitis Gilbert-Type Delta, Greece. *Basin Research*, **37**, e70014.

Romans, B.W., **Castelltort, S.**, **Covault, J.A.**, **Fildani, A.** and **Walsh, J.P.** (2016a) Environmental signal propagation in sedimentary systems across timescales. *Earth-Science Reviews*, **153**, 7–29.

Romans, B.W., **Castelltort, S.**, **Covault, J.A.**, **Fildani, A.** and **Walsh, J.P.** (2016b) Environmental signal propagation in sedimentary systems across timescales. *Earth-Science Reviews*, **153**, 7–29.

Rowley, T., **Konsoer, K.**, **Langendoen, E.J.**, **Li, Z.**, **Ursic, M.** and **Garcia, M.H.** (2021) Relationship of point bar morphology to channel curvature and planform evolution. *Geomorphology*, **375**, 107541.

Rush, A.W.D., **Kiehl, A.J.T.**, **Shields, A.C.A.** and **Zachos, A.J.C.** (2021) Increased frequency of extreme precipitation events in the North Atlantic during the PETM: Observations and theory.

Sames, B., **Wagreich, M.**, **Conrad, C.P.** and **Iqbal, S.** (2020) Aquifer-eustasy as the main driver of short-term sea-level fluctuations during Cretaceous hothouse climate phases. *Geological Society, London, Special Publications*, **498**, 9–38.

Selley, R.C. (1968) A Classification of Palaeocurrent Models. *The Journal of Geology*, **76**, 99–110.

Sharma, N., **Whittaker, A.C.**, **Watkins, S.E.**, **Valero, L.**, **Vérité, J.**, **Puigdefabregas, C.**, **Adatte, T.**, **Garcés, M.**, **Guillocheau, F.** and **Castelltort, S.** (2023) Water discharge variations control fluvial stratigraphic architecture in the Middle Eocene Escanilla formation, Spain. *Sci Rep*, **13**, 6834.

Trampush, S.M., **Huzurbazar, S.** and **McElroy, B.** (2014) Empirical assessment of theory for bankfull characteristics of alluvial channels. *Water Resources Research*, **50**, 9211–9220.

Turner, S.K. (2018) Constraints on the onset duration of the Palaeocene-Eocene Thermal Maximum. *Philos Trans A Math Phys Eng Sci*, **376**, 20170082.

Van der Meulen, S. (1989) The distribution of Pyrenean erosion material, deposited by eocene sheetflood systems and associated fan-deltas : a fossil record in the Monllobat and adjacent Castigaleu formations, in the drainage area of the present Rio Noguerra Ribagorzana, provinces of Huesca and Lérida, Spain. *Rijksuniversiteit, Mineralogisch-geologisch instituut*, Utrecht, 125 pp.

Van Eden, J.G. (1970) A reconnaissance of deltaic environment in the middle Eocene of the south-central Pyrenees, Spain, 4th edn. *GEOL. EN MIJNBOUW*.

Wang, B. and **Ding, Q.** (2008) Global monsoon: Dominant mode of annual variation in the tropics. *Dynamics of Atmospheres and Oceans*, **44**, 165–183.

Wentworth, C.K. (1922) A Scale of Grade and Class Terms for Clastic Sediments. *The Journal of Geology*, **30**, 377–392.

Westerhold, T., MarwanNorbert, **Drury, A.J.**, **Liebrand, D.**, **Agnini, C.**, **Anagnostou, E.**, **Barnet, J.**, **Bohaty, S.**, **De Vleeschouwer, D.**, **Fabio, F.**, **Frederichs, T.**, **Hodell, D.**, **Holbourn, A.**, **Kroon, D.**, **Lauretano, V.**, **Littler, K.**, **Lourens, L.**, **Lyle, M.**, **Pälike, H.** and **Zachos, J.C.** (2020) An astronomically dated record of Earth’s climate and its predictability over the last 66 million years. *Science (New York, N.Y.)*, **369**, 1383–1387.

Westerhold, T., **Röhl, U.**, **Donner, B.** and **Zachos, J.C.** (2018) Global Extent of Early Eocene Hyperthermal Events: A New Pacific Benthic Foraminiferal Isotope Record From Shatsky Rise (ODP Site 1209). *Palaeoceanography and Palaeoclimatology*, **33**, 626–642.

Westerhold, T., **Röhl, U.**, **Frederichs, T.**, **Agnini, C.**, **Raffi, I.**, **Zachos, J.C.** and **Wilkens, R.H.** (2017) Astronomical calibration of the Ypresian timescale: implications for seafloor spreading rates and the chaotic behavior of the solar system? *Climate of the Past*, **13**, 1129–1152.

Whitchurch, A.L., **Carter, A.**, **Sinclair, H.D.**, **Duller, R.A.**, **Whittaker, A.C.** and **Allen, P.A.** (2011) Sediment routing system evolution within a diachronously uplifting orogen: Insights from detrital zircon thermochronological analyses from the South-Central Pyrenees. *American Journal of Science*, **311**, 442–482.

Whittaker, A.C. (2012) How do landscapes record tectonics and climate? *Lithosphere*, **4**, 160–164.

Wolman, M.G. (1954) A method of sampling coarse river-bed material. *Eos, Transactions American Geophysical Union*, **35**, 951–956.

Wood, J., **McLeod, J.S.**, **Lyster, S.J.** and **Whittaker, A.C.** (2022) Rivers of the Variscan Foreland: fluvial morphodynamics in the Pennant Formation of South Wales, UK. *Journal of the Geological Society*, **180**, jgs2022-048.

TABLES

Parameter	**Definition**
h_{xs}	Mean cross-set height, measured as the mean from a distribution of heights measured within one cross-set
h_d	Height of the original dune, before preservation as a cross-set
h_{acc}	Height of observable accretion set within preserved barforms
H	The depth of formative water flow at the time of deposition, often assumed to represent bankfull conditions
$q_{s,w}$	Unit discharge of water or sediment at the time of deposition, measured per unit width
$Q_{s,w}$	Discharge of water of sediment, measured per individual river channel
$Q_{s,w(total)}$	Total discharge of water or sediment for all channels of the river

Table 1. Key palaeohydrological variables and definitions

	Number of barforms accreting downstream ($\Delta_{db} \leq 45°$)	Number of barforms accreting laterally ($45° < \Delta_{db} \leq 135°$)	Number of barforms accreting upstream ($\Delta_{db} > 135°$)
Castissent	45 (74%)	14 (23%)	2 (3%)
Montllobat	15 (39%)	17 (45%)	6 (16%)

Table 2. Bar-mode results from dune-bar orientation difference analysis.

FIGURES

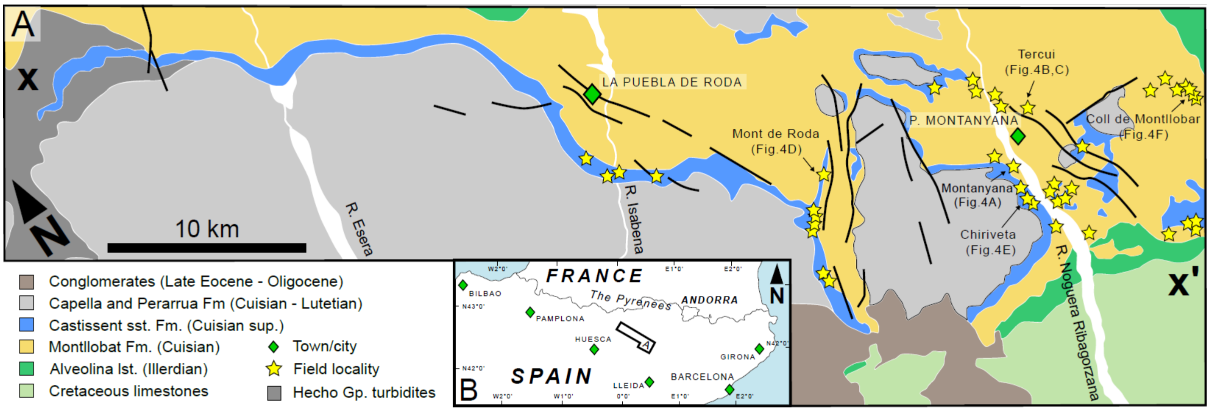

Fig 1. Study region. (A) Geologic map of field area and the Montllobat and Castissent Formations, including field localities (after Chanvry et al., 2018). Section X-X' is presented on Fig. 3. (B) Regional map, where the box is inset A.

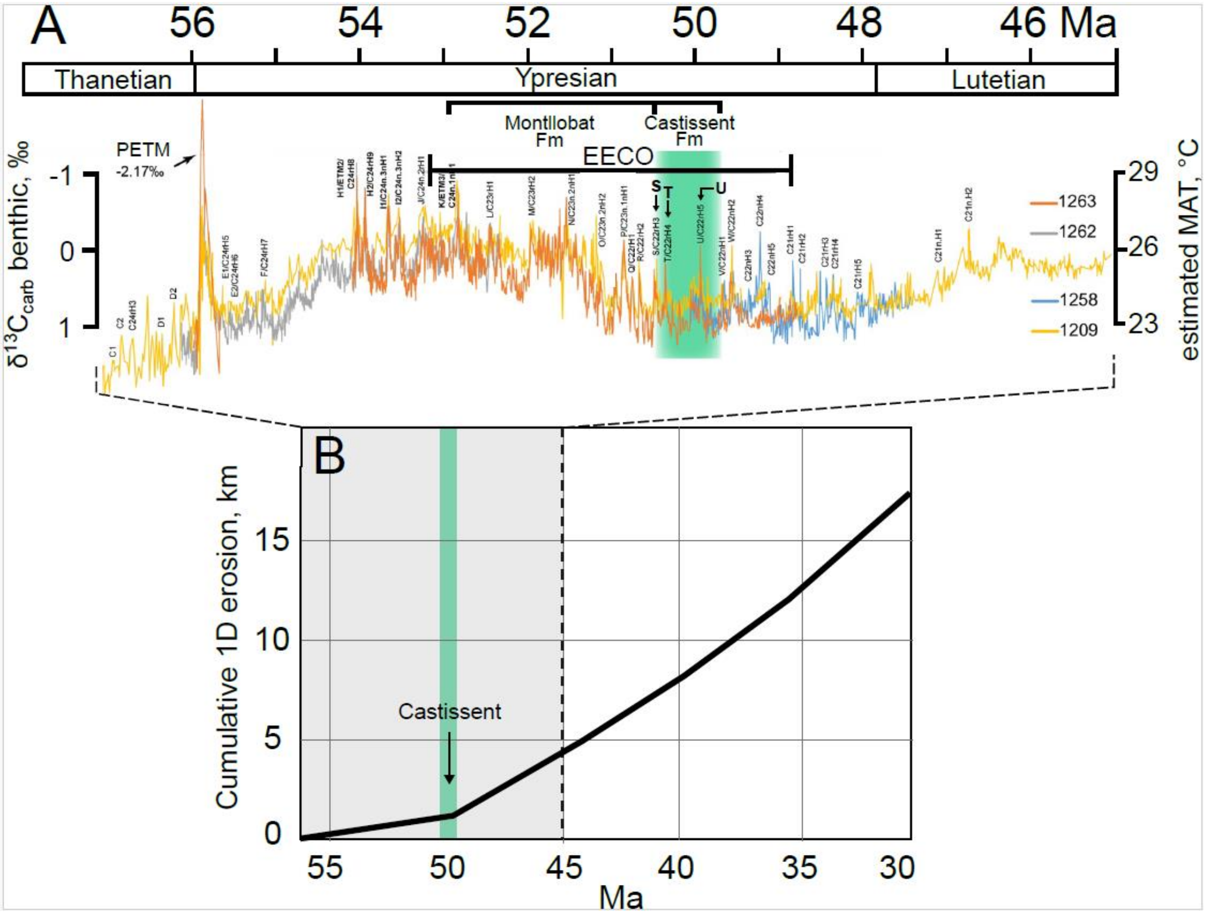

Fig 2. Tectono-climatic context of the Montllobat and Castissent Formations. (A) Benthic carbon isotope records for the upper Palaeocene and early Eocene (Honegger et al., 2020) where each coloured line represents δ13C from the IODP cores numbered on the right, and geologic timescale, with the Castissent interval highlighted in green. The mean annual temperature (MAT) change is illustrated with the axis on the right, estimated based on CO_2 output (Honegger et al., 2020). (B) Cumulative 1-D erosion in Zone 4 of the Pyrenean orogen (Curry et al., 2021), illustrating exhumation from 56 – 30 Ma.

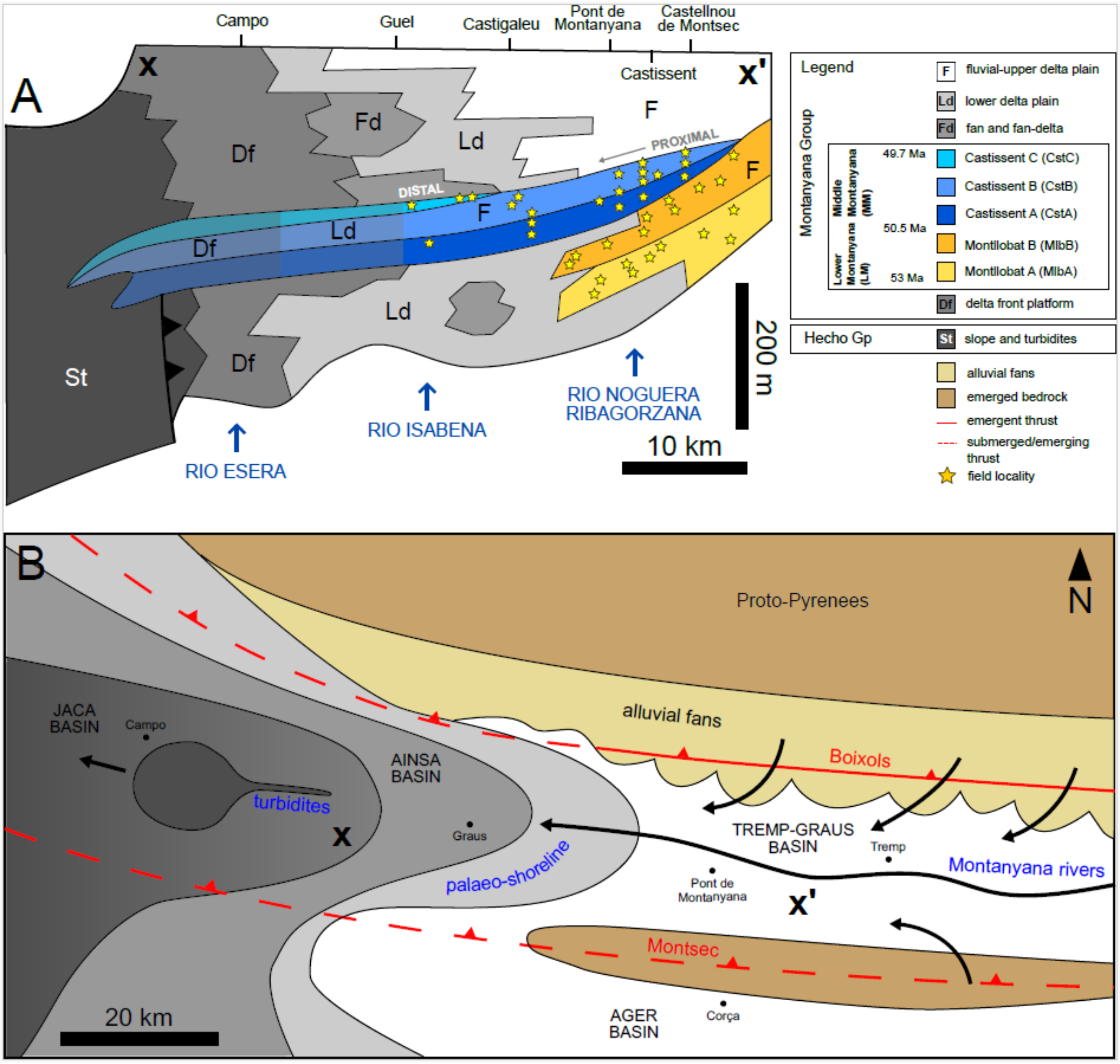

Fig 3. Stratigraphy and palaeogeography. (A) Schematic stratigraphic section, modified from Marzo (1988), from east (up-dip, X') to west (down-dip, X), showing field localities, major towns and rivers, and depositional environments. The location of section is labelled on Fig. 1A and Fig. 3B. (B) Schematic palaeogeographic map of the Montanyana sediment routing system c. 53-50 Mya, illustrating foreland sub-basins and depositional environments.

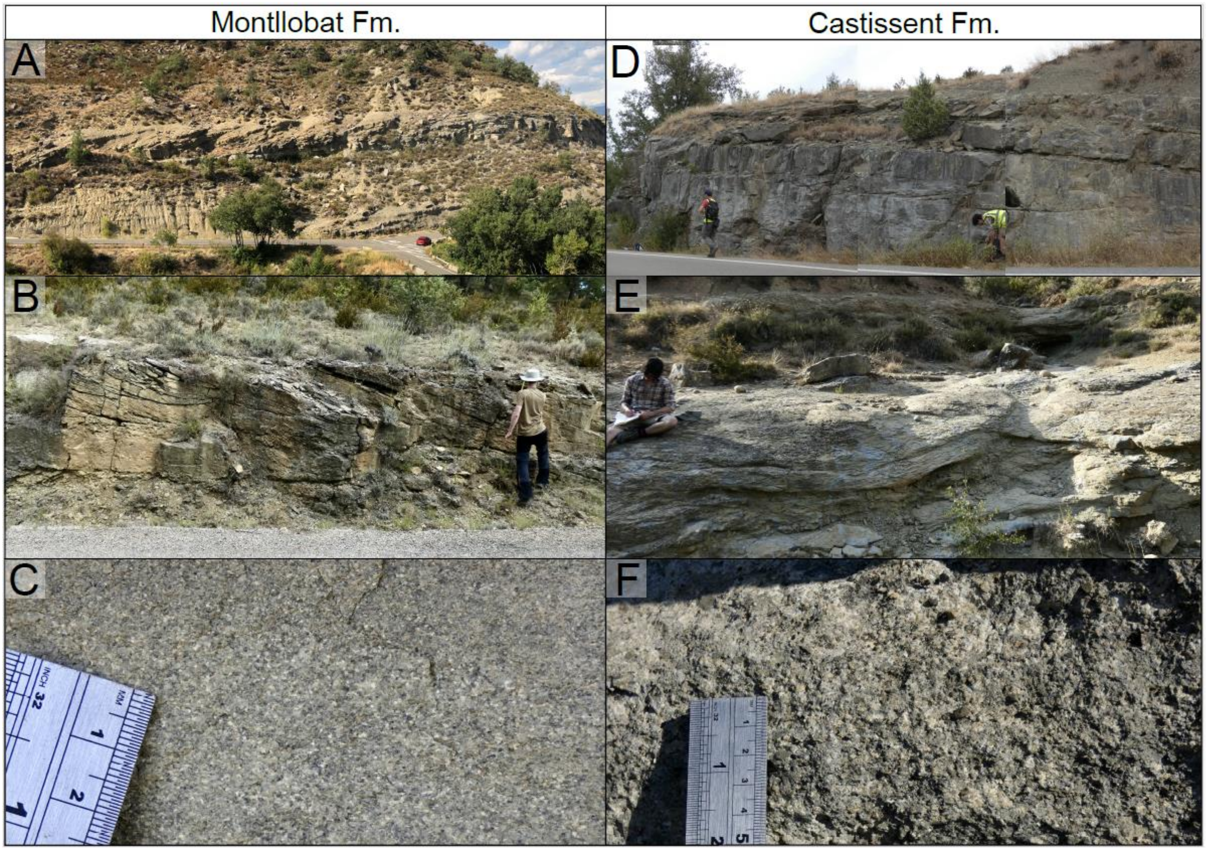

Fig. 4. The Montllobat (A-C) and Castissent (D-F) Formations at outcrop. (A) Point bar accretion sets at El Point Bar de Montanyana, (B) dune and bar-scale cross-strata near Tercui, (C) fine- to medium-grained sandstone near Tercui, (D) Amalgamated channel-fill sandstone bodies at Mont de Roda, (E) dune and bar-scale cross-strata at Chiriveta, (F) very coarse-grained sandstone near Coll de Montllobar. Locations shown on Fig. 1A.

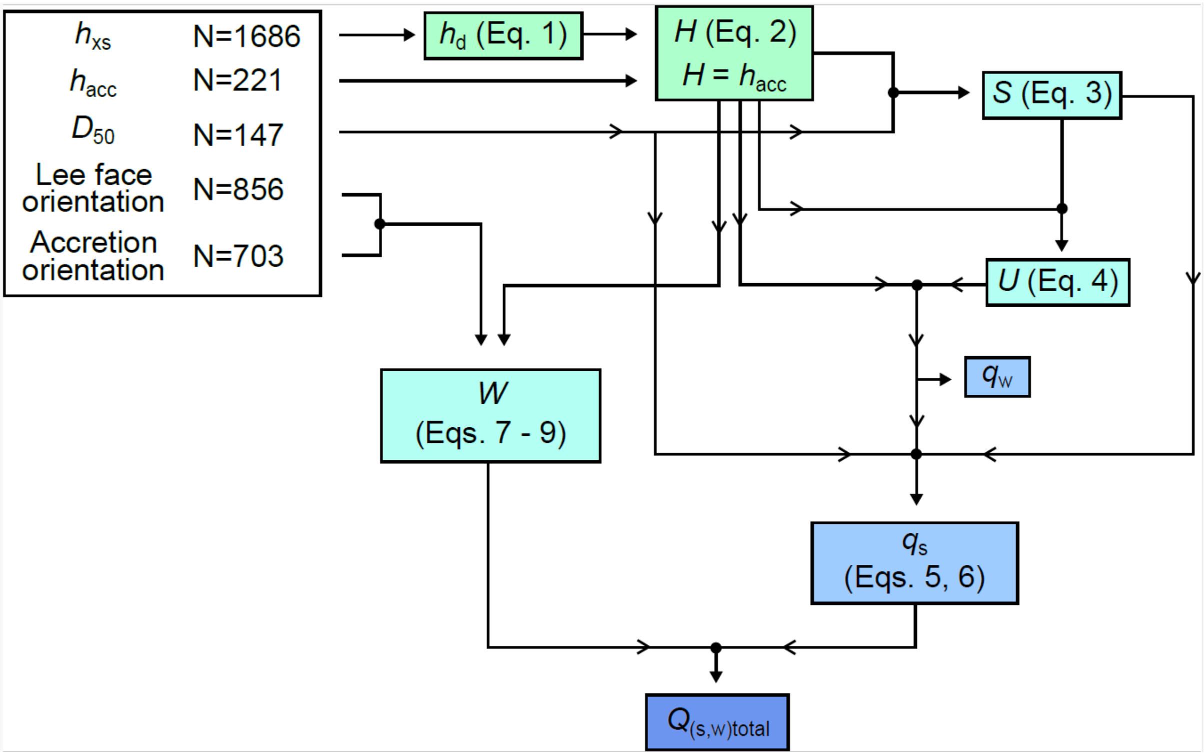

Fig. 5. Palaeohydrological workflow, from field data collection to quantitative suite of palaeohydrological approaches, where formulae used are indicated in each box. See Table 1 for definitions.

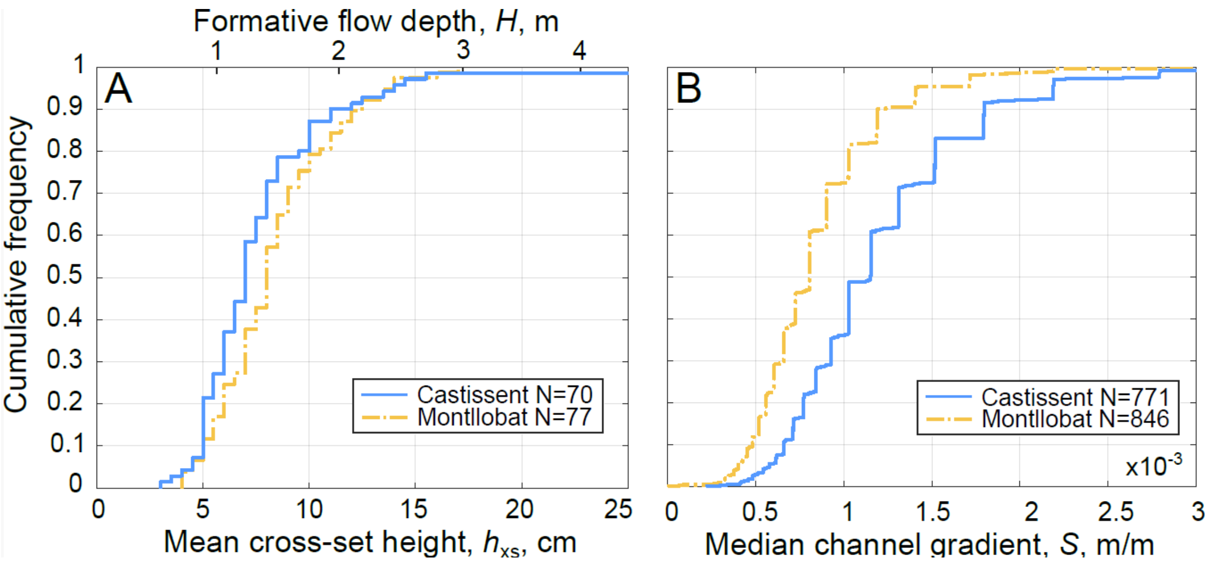

Fig. 6. Cumulative density functions (CDFs) of palaeohydrologic results. (A) CDF of mean cross-set thickness, and flow depth (calculated using Eqs. 1 and 2). (B) CDF of median channel gradient, S, calculated using Eq. 3.

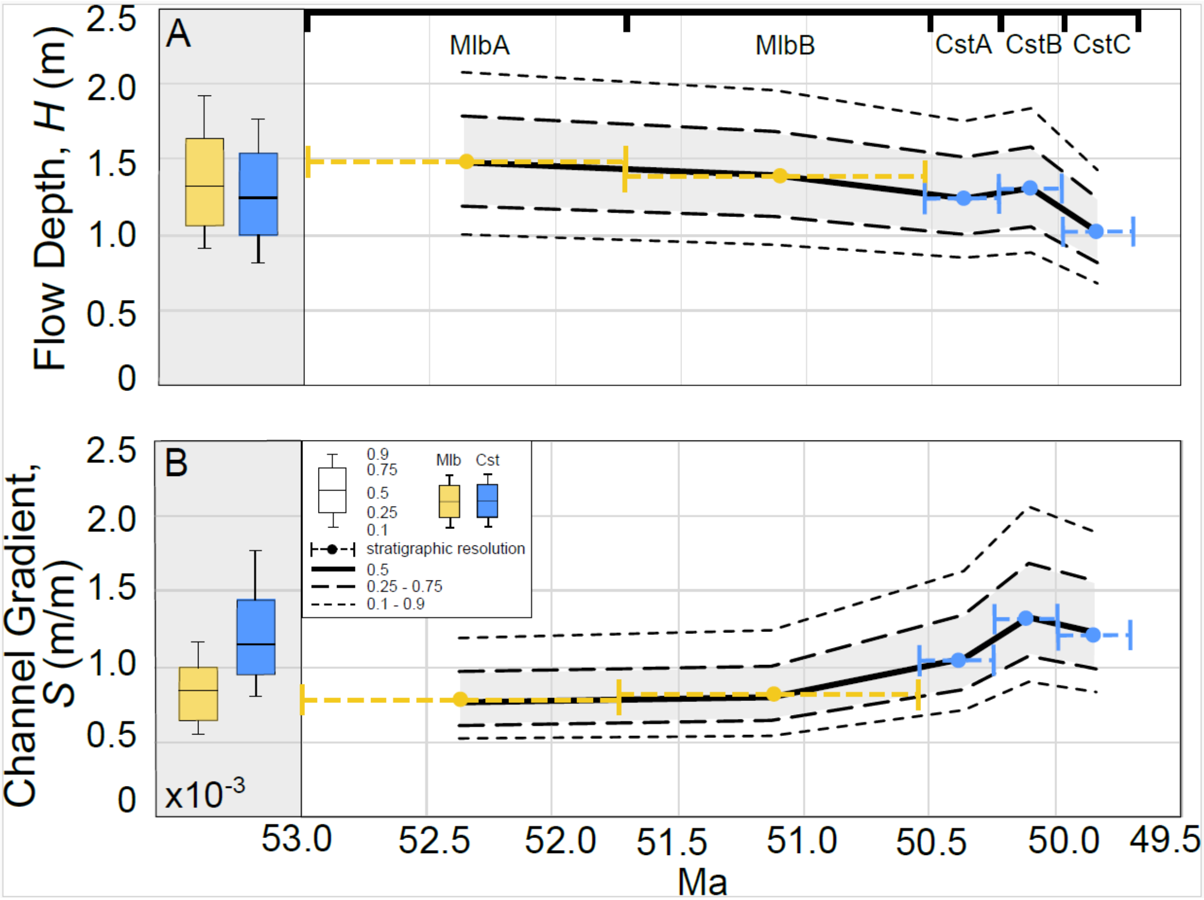

Fig. 7. Depth and slope through time. (A) Formative flow depth (bedform approach) through time. The box plots illustrate the reconstructed flow depth across each formation, and the graph depicts uncertainty in reconstructed depth for each member of the two formations. Each formation has been divided equally into its members, as timing of their constituent fluvial deposits is poorly constrained. The solid black line represents the median value of flow depth, the thick dashed lines represent the upper and lower quartiles (where the shaded region is the interquartile range), and the thin dashed lines represent the 10th and 90th percentiles. (B) As in (A) but for reconstructed palaeoslope.

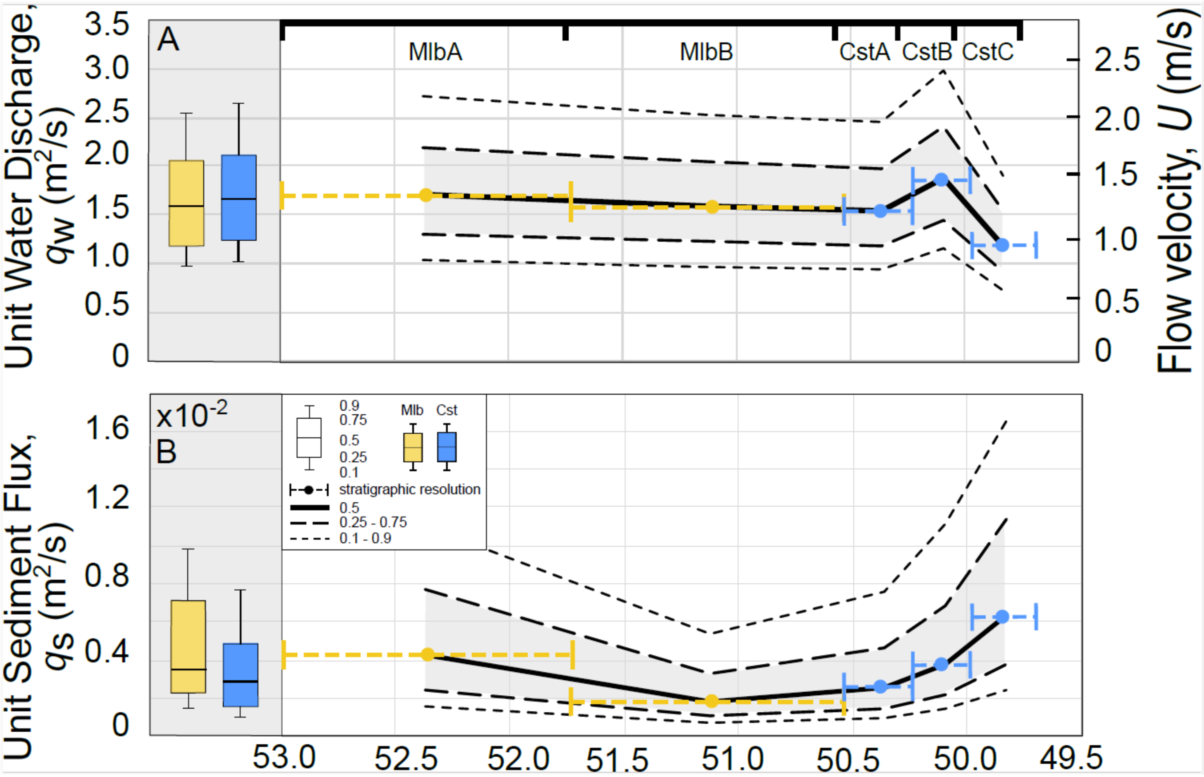

Fig. 8. Water and sediment discharge through time. (A) Unit water discharge, q_w, and flow velocity, U, through time, calculated using Eq. 4. The box plots represent the median depth within each formation, and the graph depicts uncertainty in reconstructed q_w for each Member. The solid black line represents the median value, the thick dashed lines represent the upper and lower quartiles (where the shaded region is the interquartile range), and the thin dashed lines represent the 10^{th} and 90^{th} percentiles. (B) As in (A) but for reconstructed unit sediment flux, using Eq. 5.

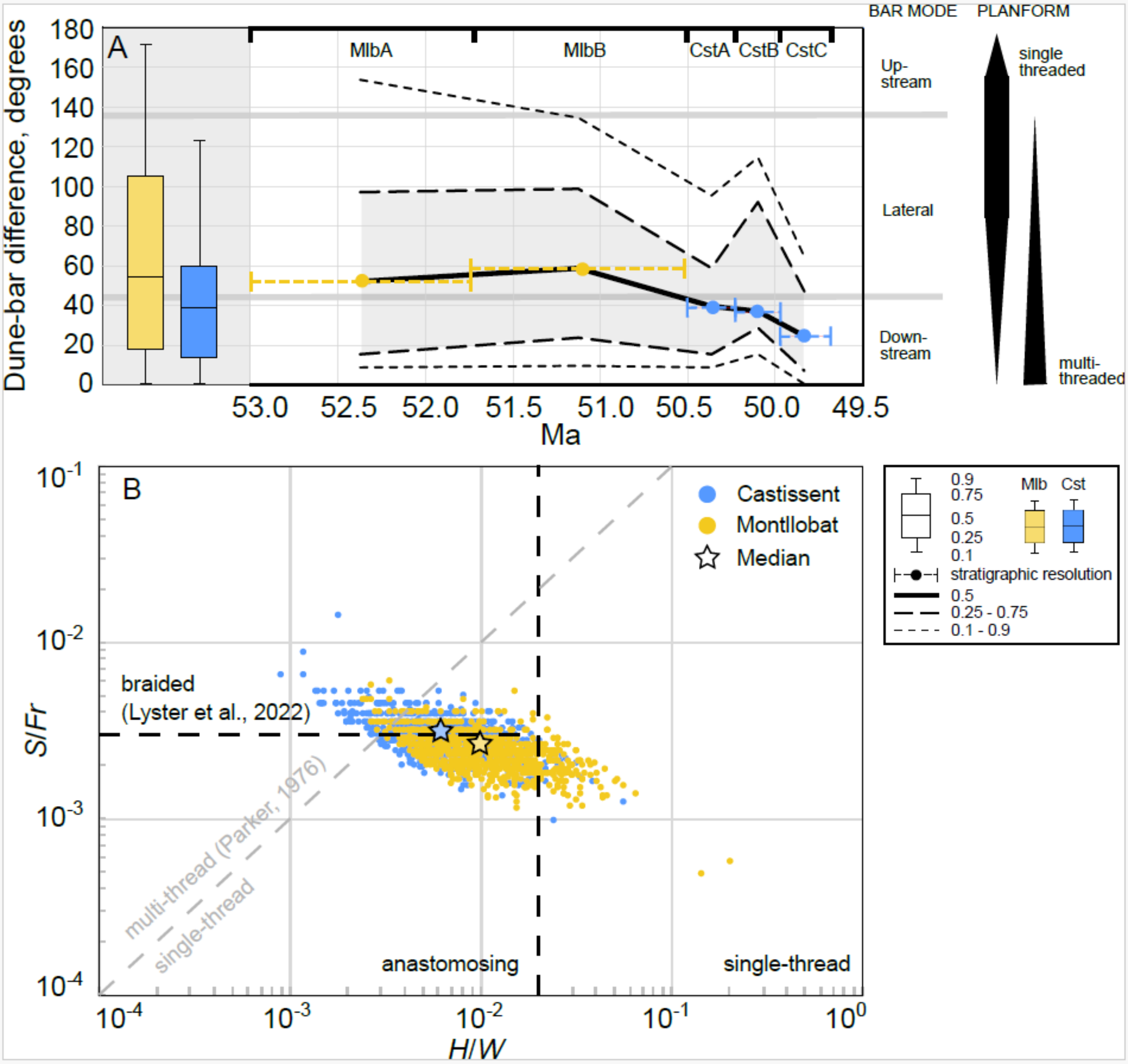

Fig. 9. Planform results. (A) Dune-bar angular difference through time, where the box plots represent the median dune-bar difference within each formation, and the graph depicts uncertainty for each Member. Where median dune-bar angular difference is between 45 and 135°, dominant bar mode is considered to be lateral. The solid black line represents the median value, the thick dashed lines represent the upper and lower quartiles (where the shaded region is the interquartile range), and the thin dashed lines represent the 10^{th} and 90^{th} percentiles. (B) Planform stability plot, where slope/Froude number is plotted against depth/width, using a random distribution of values within uncertainty for each Formation. The planform stability fields of Parker (1976) and Lyster et al. (2022) are presented in grey and black, respectively.

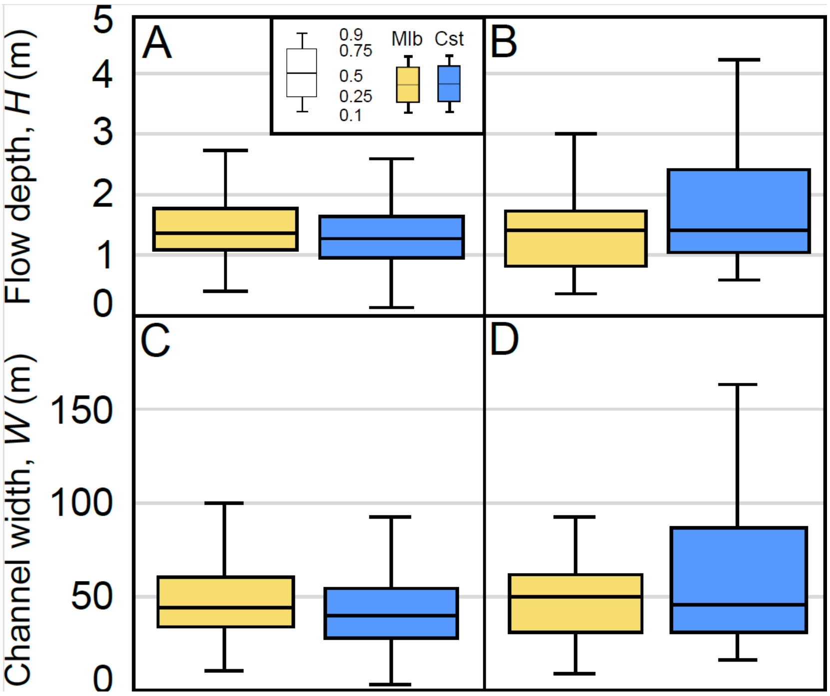

Fig. 10. Barform and bedform-based estimates of depth and width. (A) Boxplots illustrating flow depth results from the bedform approach, and (B) from the barform approach. (C) Channel width estimates (Eq. 8) using depths from the bedform approach, and (D) from the barform approach. Median width and depth values are comparable for each approach.

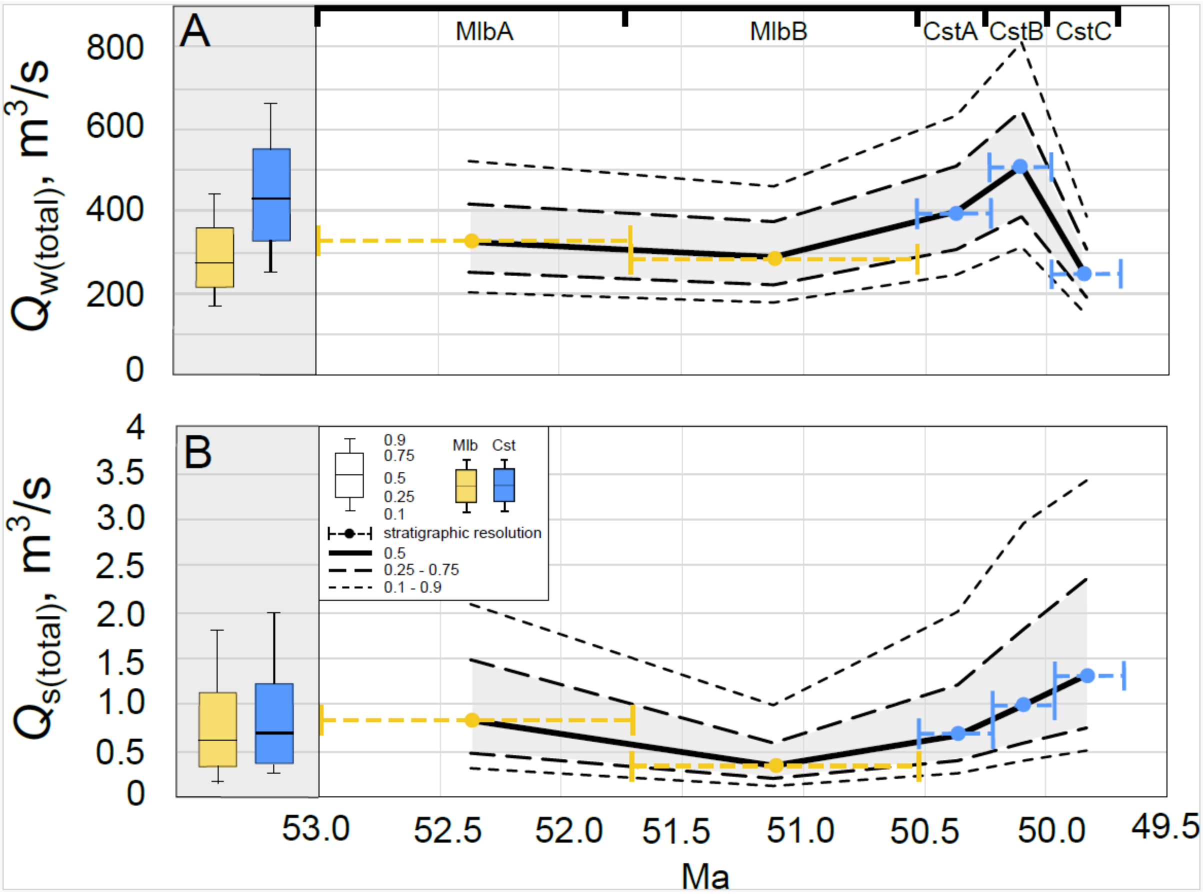

Fig 11. Total fluxes. (A) The total water discharge, $Q_{w(total)}$, and (B) the total sediment discharge, $Q_{s(total)}$. The solid black line represents the median value, the thick dashed lines represent the upper and lower quartiles (where the shaded region is the interquartile range), and the thin dashed lines represent the 10th and 90th percentiles.

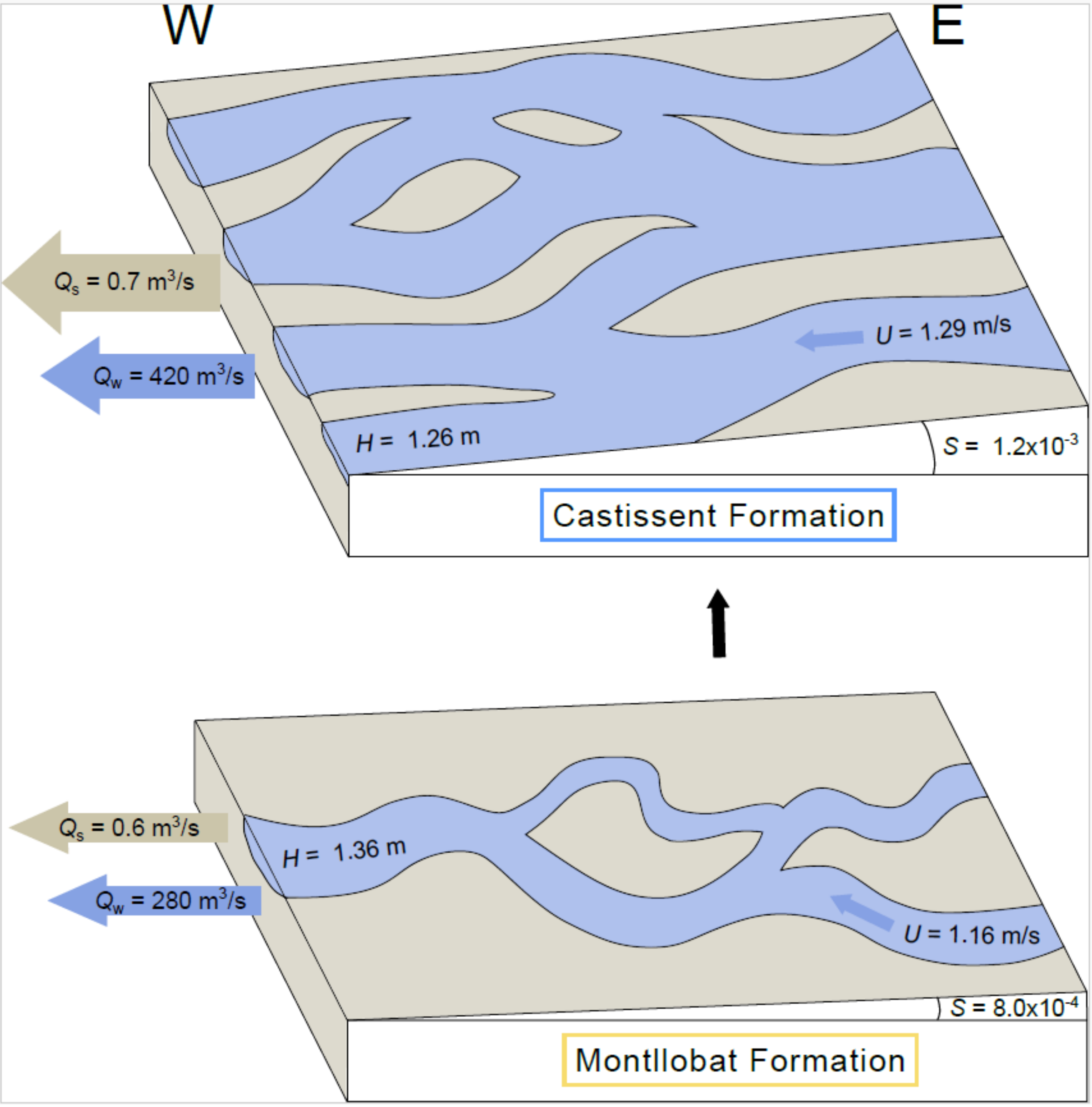

Fig. 12. Schematic diagram illustrating changing palaeoslope, flow velocity, depth, planform, and total water and sediment flux from the Montllobat to the Castissent Formation. Some values are not to scale.